JBC ARTICLE

Efficient farnesylation of an extended C-terminal C(x)$_3$$X$ sequence motif expands the scope of the prenylated proteome

Received for publication, July 10, 2017, and in revised form, December 24, 2017 Published, Papers in Press, December 27, 2017, DOI 10.1074/jbc.M117.805770

Melanie J. Blanden[‡], Kiall F. Suazo[§], Emily R. Hildebrandt[¶], Daniel S. Hardgrove[¶], Meet Patel[¶], William P. Saunders[¶], Mark D. Distefano[§], Walter K. Schmidt[¶], and James L. Hougland[‡1]

From the [‡]Department of Chemistry, Syracuse University, Syracuse, New York 13244, the [§]Department of Chemistry, University of Minnesota, Minneapolis, Minnesota 55455, and the [¶]Department of Biochemistry and Molecular Biology, University of Georgia, Athens, Georgia 30602

Edited by Henrik G. Dohlman

Protein prenylation is a post-translational modification that has been most commonly associated with enabling protein trafficking to and interaction with cellular membranes. In this process, an isoprenoid group is attached to a cysteine near the C terminus of a substrate protein by protein farnesyltransferase (FTase) or protein geranylgeranyltransferase type I or II (GGTase-I and GGTase-II). FTase and GGTase-I have long been proposed to specifically recognize a four-amino acid *CAAX* C-terminal sequence within their substrates. Surprisingly, genetic screening reveals that yeast FTase can modify sequences longer than the canonical *CAAX* sequence, specifically C(x)$_3$$X$ sequences with four amino acids downstream of the cysteine. Biochemical and cell-based studies using both peptide and protein substrates reveal that mammalian FTase orthologs can also prenylate C(x)$_3$$X$ sequences. As the search to identify physiologically relevant C(x)$_3$$X$ proteins begins, this new prenylation motif nearly doubles the number of proteins within the yeast and human proteomes that can be explored as potential FTase substrates. This work expands our understanding of prenylation's impact within the proteome, establishes the biologically relevant reactivity possible with this new motif, and opens new frontiers in determining the impact of non-canonically prenylated proteins on cell function.

Post-translational modification of proteins is essential for biological functions such as cell signaling and regulation of enzyme activity (1). Among the extensive and growing catalog of known post-translational modifications, protein lipidation (*e.g.* prenylation, palmitoylation, and myristoylation) can influence protein trafficking to and interaction with cellular membranes (1–9). Prenylation involves the covalent attachment of a hydrophobic isoprenoid group, either a 15-carbon farnesyl or 20-carbon geranylgeranyl group, to the side-chain thiol of a cysteine near the C terminus of certain proteins (10–12). The sequence context of this cysteine residue determines the enzyme responsible for its modification, with a cysteine within a C-terminal *CAAX* sequence recognized by protein farnesyltransferase (FTase)[2] or protein geranylgeranyltransferase type I (GGTase-I) (11, 13–17). Alternatively, a cysteine present in a C-terminal *CC* or *CXC* motif can be modified by protein geranylgeranyltransferase type II (GGTase-II), also known as Rab GGTase (18–20). Cysteine prenylation alters the biophysical properties of proteins in several well-studied cases (*e.g.* Ras and Ras-related GTPases), resulting in protein association with cell membranes where these lipidated proteins are involved in cell-signaling pathways (21–25).

The prenylation pathway involving FTase or GGTase-I consists of a number of modification steps that can precede substrate protein localization to cellular membranes (Fig. 1). In the obligate first step of this pathway, FTase or GGTase-I catalyzes cysteine alkylation with a farnesyl or geranylgeranyl group using farnesyl diphosphate (FPP) or geranylgeranyl diphosphate (GGPP), respectively. Following modification by FTase or GGTase-I, prenylated proteins bearing *CAAX* motifs are often subject to additional modifications involving the *CAAX* sequence amino acids (26–29). Proteolytic removal of the last three *-AAX* amino acids by membrane-associated proteases Rce1p or Ste24p results in a C-terminal prenylcysteine residue bearing a negatively charged carboxylate group. This carboxylate moiety is then methylated by the *S*-adenosylmethionine-dependent enzyme isoprenylcysteine carboxyl methyltransferase. All three modification steps are necessary for many prenylated proteins to function optimally, although there can be variation in the extent of, and dependence on, these subsequent modifications (30, 31). Recently, a shunt pathway for prenylated proteins in yeast has been reported in which prenyla-

This work was supported by National Institutes of Health Grants GM084152 (to M. D. D.) and GM117148 (to W. K. S.) and Department of Education Graduate Assistance in Areas of National Need (GAANN) Fellowship P200A090277 (to M. J. B.). The authors declare that they have no conflicts of interest with the contents of this article. The content is solely the responsibility of the authors and does not necessarily represent the official views of the National Institutes of Health.

This article contains Figs. S1–S3 and Tables S1–S4.

[1] To whom correspondence should be addressed. Tel.: 315-443-1134; Fax: 315-443-4070; E-mail: hougland@syr.edu.

[2] The abbreviations used are: FTase, farnesyltransferase; GGTase, geranylgeranyltransferase; TCEP, tris(2-carboxyethyl)phosphine; eGFP, enhanced GFP; Dns/dansyl, 5-dimethylaminonaphthalene-1-sulfonyl; TAMRA, tetramethylrhodamine; RP-HPLC, reverse-phase HPLC; CFU, colony-forming unit; FDR, false discovery rate; oligo, oligonucleotide; FPP, farnesyl diphosphate; GPP, geranylgeranyl diphosphate; LC-MS, liquid chromatography-mass spectrometry; MS/MS, tandem mass spectrometry; ESI, electrospray ionization; TMT, tandem mass tag; CuAAC, Cu(II)-catalyzed alkyne-azide cycloaddition; TEAB, triethylammonium bicarbonate.

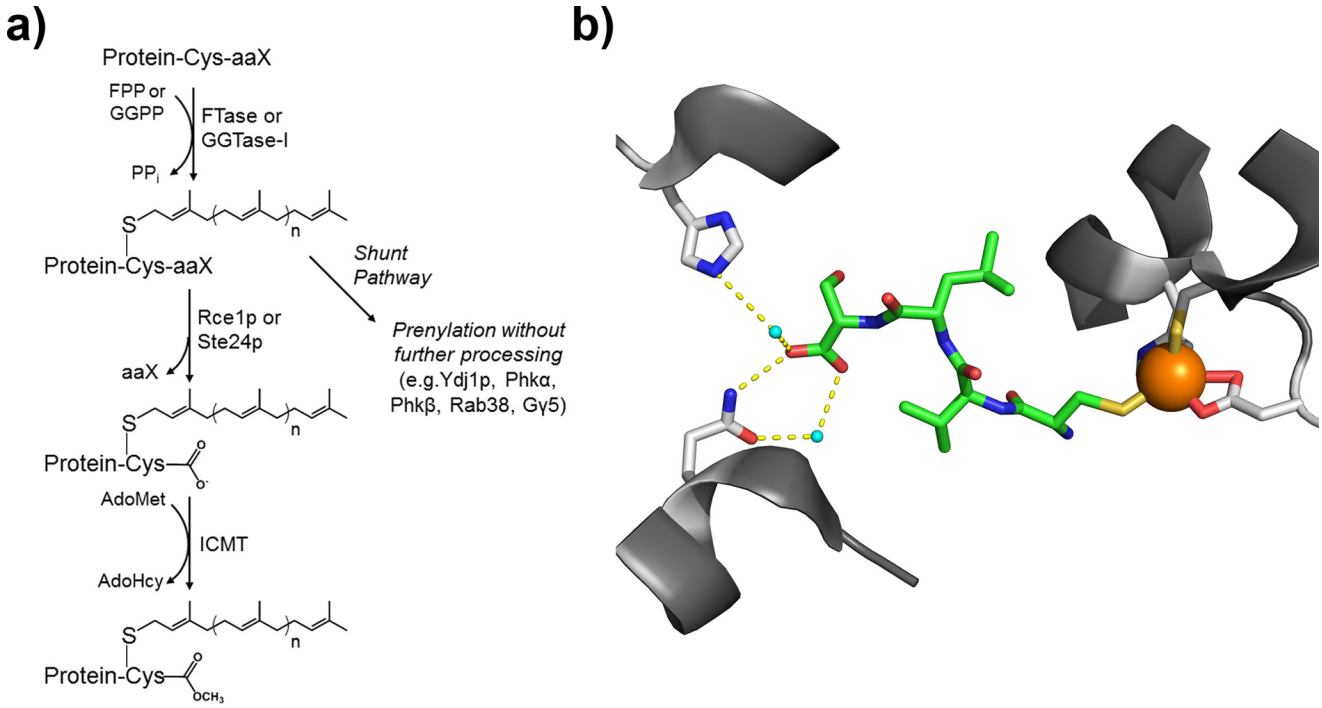

Figure 1. Prenylation pathway recognition and modification of proteins terminating in *CAAX* sequences. *a,* protein modification steps observed within the prenylation pathway, including a shunt pathway for proteins undergoing only prenylation without subsequent proteolysis (32). *b,* structural model of FTase recognition of a CVLS substrate sequence. Recognition of the length of the CVLS tetrapeptide (*green*) involves coordination of the cysteine side chain thiol to the catalytic zinc ion (*orange sphere*) and both direct and water-mediated (*teal spheres*) hydrogen bonding between the peptide C-terminal carboxylate group to FTase residues in both the α (Q167α) and β (H149β) enzyme subunits. Image was generated from Protein Data Bank code 1TN8 using PyMOL (77).

tion is the end point of *CAAX* protein modification. In this case, post-prenylation processing is not required and is actually deleterious to protein function (32).

The *CAAX* motif that has served as the *de facto* consensus motif for prenylation by FTase and GGTase-I was first described over 3 decades ago, when yeast mating factors, Ras GTPases, and nuclear lamins were found to be lipid-modified (33–38). Although there were limited early investigations into shorter *CXX* motifs (39), investigation of the *CAAX* sequence has predominantly focused on amino acid selectivity within the motif for recognition by FTase and/or GGTase-I. Biochemical and cell-based studies, including single amino acid mutations at each position of the *CAAX* sequence and reengineering of FTase and GGTase-I substrate selectivity, have contributed to the development of rules for prenyltransferase selectivity at each amino acid position within the *CAAX* sequence (11, 16, 17, 39–44). Crystallographic studies provide a valuable structural context for consideration of FTase and GGTase-I substrate selectivity (45). In addition to implicating certain FTase and GGTase-I residues as interacting with the *CAAX* substrate sequence side chains, the structural models of FTase and GGTase-I revealed contacts to the cysteine and terminal carboxylate group of the *CAAX* sequence that explain the observed preference for the four-amino acid *CAAX* substrate sequence (Fig. 1). Proteomic studies utilizing chemically modified prenyl donors, bioinformatics analysis, and computational/docking approaches have further extended our ability to identify and predict which *CAAX* motifs likely serve as substrates for FTase and/or GGTase-I (46–49).

In the expansion of our understanding of FTase and GGTase-I substrate recognition, the creation of a novel thermotolerance screen for protein prenylation in yeast has augmented our ability to leverage yeast genetic methodology to identify prenyltransferase substrate sequences (32). This screen is based on the yeast protein Ydj1p, a cytosolic type I Hsp40 co-chaperone that is required for high-temperature growth (50–53). Ydj1p is a shunted *CAAX* protein, being farnesylated but not proteolyzed and methylated (32). This crucial feature has allowed direct investigation of protein prenylation without the requirement for concurrent sequence compatibility with Rce1p or Ste24p for subsequent proteolysis.

In this work, we describe the discovery of a five-amino acid C(*x*)$_3$*X* sequence motif recognized by both yeast and mammalian FTase orthologs. Multiple C(*x*)$_3$*X* peptide sequences, originally identified by genetic screening in yeast, can be efficiently farnesylated in both peptide and protein substrates. We demonstrate that several additional C(*x*)$_3$*X* sequences derived from human proteins are efficiently prenylated by rat FTase and that a reporter protein terminating in a C(*x*)$_3$*X* sequence exhibits sufficient reactivity to be farnesylated under biologically relevant conditions within a human cell.

Results

Yeast genetic screens suggest C(x)$_3$X sequences can be prenylated by yeast FTase

Although the four-amino acid *CAAX* sequence has been widely accepted as the model for FTase and GGTase-I substrate selectivity, our investigation into the prenylation of C(*x*)$_3$*X* sequences was prompted in part by the observation that the CGGDD sequence of human annexin A2 and annexin A3 was identified as potentially prenylated in studies using *in vivo*

Table 1
Mammalian FTase reactivity with C(*x*)$_3$*X* sequences derived from yeast a-factor and thermotolerance screening

Peptide sequence	Reporter/source	Fluorescence enhancement of Dns-GC(x_3)X[a]	HPLC detection of farnesylated Dns-GC(x_3)X
CGGDD	(55, 56)	−	−
CMIIM	**a**-Factor	+	+
CVLMM	**a**-Factor	Not determined	Not determined
CAVGP	Ydj1	+	+
CAYVL	Ydj1	+	+
CCAGH	Ydj1	Not determined	Not determined
CFFYI	Ydj1	+	+
CFNSL	Ydj1	−	+
CIPVQ	Ydj1	−	+
CLPIV	Ydj1	−	+
CQGFL	Ydj1	−	+
CSIQG	Ydj1	+	+
CSRLQ	Ydj1	−	+
CSSLQ	Ydj1	−	+
CVSFG	Ydj1	−	+
CWAGG	Ydj1	−	+
CWGEV	Ydj1	−	+
CWGGA	Ydj1	−	+

[a] Activity in the fluorescence-based screening was determined by >5-fold enhancement of prenylation reaction compared with a negative control reaction, as described under "Experimental procedures."

farnesylation probes, although this reactivity was not supported by *in vitro* fluorescence-based peptide reactivity studies (54–56). This observation suggests prenylation and associated processing may be compatible with sequences of non-canonical length. To examine this possibility, we initially used yeast **a**-factor as a highly sensitive genetic reporter to identify whether C(*x*)$_3$*X* sequences could serve as prenylation motifs. Farnesylated **a**-factor is a secreted, diffusible signaling molecule produced by *MAT***a** haploid yeast that temporarily triggers cell cycle G_1 arrest in nearby *MATα* haploid yeast so that mating can occur; this arrest is enhanced in certain mutant backgrounds (*e.g. MATα sst2–1*) (57). We took advantage of the **a**-factor-induced growth arrest phenotype to screen a plasmid-based library of **a**-factor mutants with C-terminal C(*x*)$_3$*X* sequences. Through standard colony replica techniques, a plate containing a population of *MAT***a** colonies expressing mutants was printed onto a thin lawn of *MATα sst2-1* yeast; the printed plate was incubated for a period of time; individual colonies surrounded by a zone of *MATα* growth inhibition (*i.e.* halo) were scored as positive hits; and associated plasmids were recovered and sequenced. We estimate 22.5% of the possible C(*x*)$_3$*X* combinations were evaluated (*i.e.* ~40,000 colonies; see "Experimental procedures" for description of coverage estimate) (58). With this limited coverage of the potential sequence space, the **a**-factor screen yielded two C(*x*)$_3$*X* hits (Table 1). The two C(*x*)$_3$*X* sequences were retested with other **a**-factor mutant sequences using the halo assay (Fig. 2*a*). The halos associated with the C(*x*)$_3$*X* sequences were qualitatively smaller than those associated with wildtype **a**-factor (CVIA C-terminal sequence). Unexpectedly, the CGGDD sequence did not produce a halo; this was true even when encoding the mutant in an overexpression vector. Of note, the halo associated with **a**-factor "CASQ," which has a Rce1p/Ste24p *CAAX* protease cleavage-resistant motif that severely compromises **a**-factor production (~1–2% relative to CVIA), still produced a halo similar to wildtype (32). This is due to the halo assay acting as an extremely sensitive and qualitative method for measuring **a**-factor production. To better assess the amounts of **a**-factor produced by mutants, we used a quantitative mating assay. We determined the C(*x*)$_3$*X* sequences promoted far fewer mating events relative to that observed for the wildtype and cleavage-resistant **a**-factor (Fig. 2*a*, numerical values *below* each panel). The reduced production of mature **a**-factor with the C(*x*)$_3$*X* hit sequences and the lack of production with CGGDD could reflect deficiencies in either prenylation and/or proteolysis as both modification steps are required to yield fully active **a**-factor.

To complement and expand upon the **a**-factor screen, we used the Ydj1p Hsp40 chaperone as an independent genetic reporter to select for C(*x*)$_3$*X* motifs compatible with farnesylation by yeast FTase. For proper function and support of yeast growth at elevated temperatures, Ydj1p requires cysteine farnesylation but does not require subsequent proteolytic and carboxylmethylation modifications typically associated with prenylated C*AAX* proteins. The Ydj1p-based approach provided several advantages over the **a**-factor screen, including higher throughput based on a temperature-sensitive selection and elimination of the requirement for downstream proteolysis and carboxylmethylation following prenylation (32, 50). Through this approach, effects on thermotolerance can be directly related to changes in sequence modification by FTase rather than impact on downstream processing steps. A library of Ydj1p mutants with C(*x*)$_3$*X* sequences was expressed in yeast, and individual colonies surviving growth at high temperature were identified. Based on codon redundancy and the number of colonies examined (~125,000), we estimate 48% of possible C(*x*)$_3$*X* sequences were evaluated (58). The screen yielded 15 C(*x*)$_3$*X* sequence hits (Table 1). The Ydj1p C(*x*)$_3$*X* hits support growth at high temperature similar to wildtype Ydj1p (CASQ C-terminal sequence). They are more effective than Ydj1p appended with the CVIA sequence that is cleaved by Rce1p and Ste24p, the CMIIM and CVLMM sequences that were derived from **a**-factor-based screening, and the annexin A2 CGGDD sequence identified by proteomics studies (Fig. 2*B*). The thermotolerant Ydj1p C(*x*)$_3$*X* mutants were subsequently analyzed for evidence of prenylation by a mobility shift assay. In this assay, farnesylated Ydj1p has increased SDS-PAGE mobility relative to the unprenylated protein, which can be produced by expression in an FTase-deficient yeast strain (*i.e. ram1*). Using this assay, all C(*x*)$_3$*X* hits identified by Ydj1p-based screening exhibited prenylation, albeit only partially in

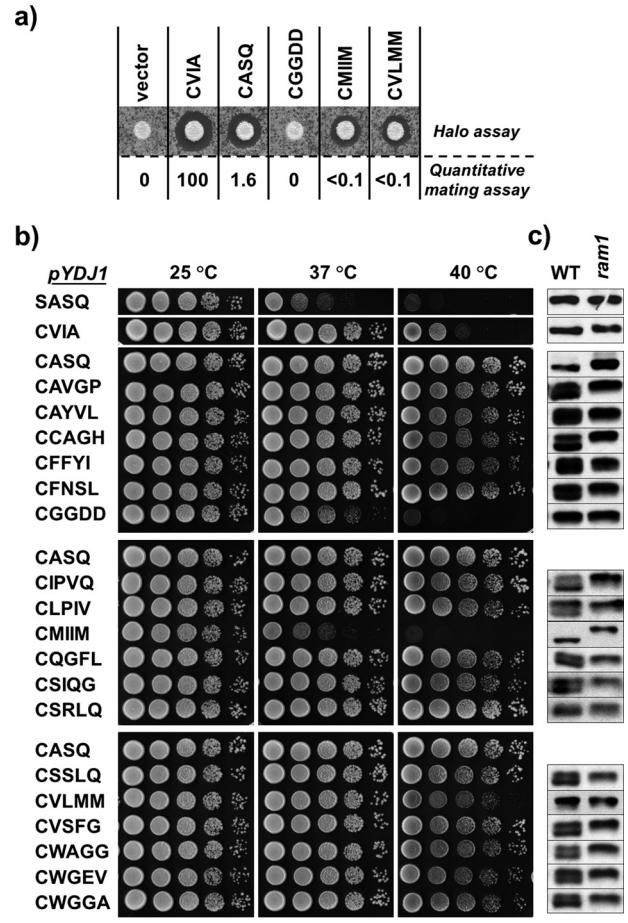

Figure 2. Phenotypes and isoprenylation status of C(*x*)$_3$*X* motifs identified by yeast-based screening. *a,* **a**-factor C(*x*)$_3$*X* variants encoded in *CEN LEU2* plasmids and transformed into SM2331 (*MAT***a** *mfa1 mfa2*) were evaluated for their ability to produce **a**-factor using a spot halo assay; the CGGDD variant was encoded in a high-copy *2μ URA3* plasmid but otherwise treated identically. Strains were spotted onto YPD, cultured for 48 h at 30 °C, and replica-transferred onto a thin lawn of RC757 (*MATα sst2-1*). Plates were imaged after 16 h of incubation at 30 °C. The same strains were subjected to quantitative mating analyses, which yielded the numerical values indicated *below* each image, where values are reported as percent relative to control (CVIA). *b,* Ydj1p C(*x*)$_3$*X* variants encoded in low-copy *CEN* plasmids were evaluated for their ability to rescue growth of yWS304 (*ydj1*Δ) at indicated temperatures. Each set of spots represents a 10-fold dilution series prepared from a saturated culture grown in selective media that was spotted onto YPD. Images are representative of data from two separate experiments in which at least two replicates of each strain were evaluated. *c,* immunoblot of lysates from strains containing the indicated Ydj1p C(*x*)$_3$*X* variant. Farnesylated Ydj1p has increased mobility compared with unmodified Ydj1p. The strains used were yWS304 (*WT*) and yWS1632 (*ram1*); *RAM1* encodes the FTase β subunit.

most cases (Fig. 2*c*). Of note, the CMIIM sequence appeared to be completely modified in the context of Ydj1p. By contrast, the CGGDD sequence did not appear to be modified.

Mammalian protein prenyltransferase activity with C(x)$_3$X peptide substrates

Although these yeast experiments support the notion that prenylation of proteins terminating in C(*x*)$_3$*X* sequences occurs within yeast cells, these studies do not conclusively establish that the C(*x*)$_3$*X* motif can serve as a substrate for FTase or GGTase-I within yeast. For example, the identified C(*x*)$_3$*X* sequences could be processed by a carboxypeptidase to yield a shorter canonical *CAAX* sequence. This type of proteolytic "trimming" prior to modification by a prenyltransferase would present a new step within the established prenylation pathway, but it would not reflect an expanded sequence length tolerance for the protein prenyltransferases. To address this ambiguity, we investigated the prenylation of C(*x*)$_3$*X* sequences in the context of synthetic peptides using purified mammalian FTase and GGTase-I in cell-free prenylation assays. These assays eliminate the possibility of peptide substrate processing and examine whether the reactivity with C(*x*)$_3$*X* sequences is a general feature of these enzymes or is exclusive to the yeast orthologs.

For these assays, 15 C(*x*)$_3$*X* sequences identified by yeast screening were synthesized as 6-mer peptides with each C(*x*)$_3$*X* sequence preceded by a glycine residue with a pendant N-terminal dansyl fluorophore (Dns-GC(*x*)$_3$*X*) (Table 1). As demonstrated in previous studies using canonical *CAAX* sequence peptides, attachment of the environmentally sensitive dansyl fluorophore allows real-time monitoring of prenylation through dansyl group fluorescence enhancement upon peptide prenylation (59–62). Using this assay, incubation with rat FTase and FPP resulted in significant fluorescence enhancement (>5-fold, relative to negative "−FPP" control) with 5 of the 15 sequences (Fig. 3*a* and Table 1). Among these sequences, two peptides (Dns-GCMIIM and Dns-GCAVGP) exhibited a plateau in fluorescence consistent with complete farnesylation within 4 h (Fig. 3*b*). In parallel reactions with rat GGTase-I and GGPP, none of the Dns-GC(*x*)$_3$*X* peptides exhibited an increase in fluorescence suggesting no geranylgeranylation activity. Notably, the annexin CGGDD sequence was also evaluated and observed to be unreactive under all conditions tested.

To confirm that the observed increase in fluorescence with Dns-GC(*x*)$_3$*X* peptides reflects peptide prenylation, samples generated using peptide incubation with FTase/FPP and GGTase-I/GGPP were analyzed by reverse-phase HPLC (RP-HPLC) to directly detect the prenylated peptide product. This method detects prenylation by a shift in retention time for the prenylated product compared with the unmodified substrate (43, 63). As expected from the fluorescence enhancement assay, the Dns-GCMIIM and Dns-GCAVGP peptides were completely farnesylated as reflected by the disappearance of the substrate peak and appearance of a new peak at a longer retention time (Fig. 3*c*). Farnesylation of Dns-GCMIIM and Dns-GCAVGP was further confirmed by LC-MS/MS, with peaks at 1104.4 and 940.5 Da for Dns-GCMIIM and Dns-GCAVGP, respectively, corresponding to their predicted masses when modified with a 204-Da farnesyl group. There was no detection of the non-farnesylated substrates (Dns-GCMIIM, 899.5 Da and Dns-GCAVGP, 735.3 Da) (Fig. 3*d*). The observed MS/MS fragments were consistent with the calculated a- and b-type ions of the farnesylated peptides (Table S2). In addition, the characteristic fragments from the loss of thiofarnesyl moiety (b3* and b4*) were detected. This is a result of the side-chain cleavage between the cysteine β-carbon and sulfur atom, indicating the farnesyl group was indeed appended to cysteine (64).

Surprisingly, 13 of the 14 remaining Dns-GC(*x*)$_3$*X* peptides (all except for Dns-GCGGDD) exhibited formation of the farnesylated product when monitored by RP-HPLC, with Dns-GCWGEV and Dns-GCQGFL showing nearly quantitative modification (Table 1 and Fig. S2). Although a small number of

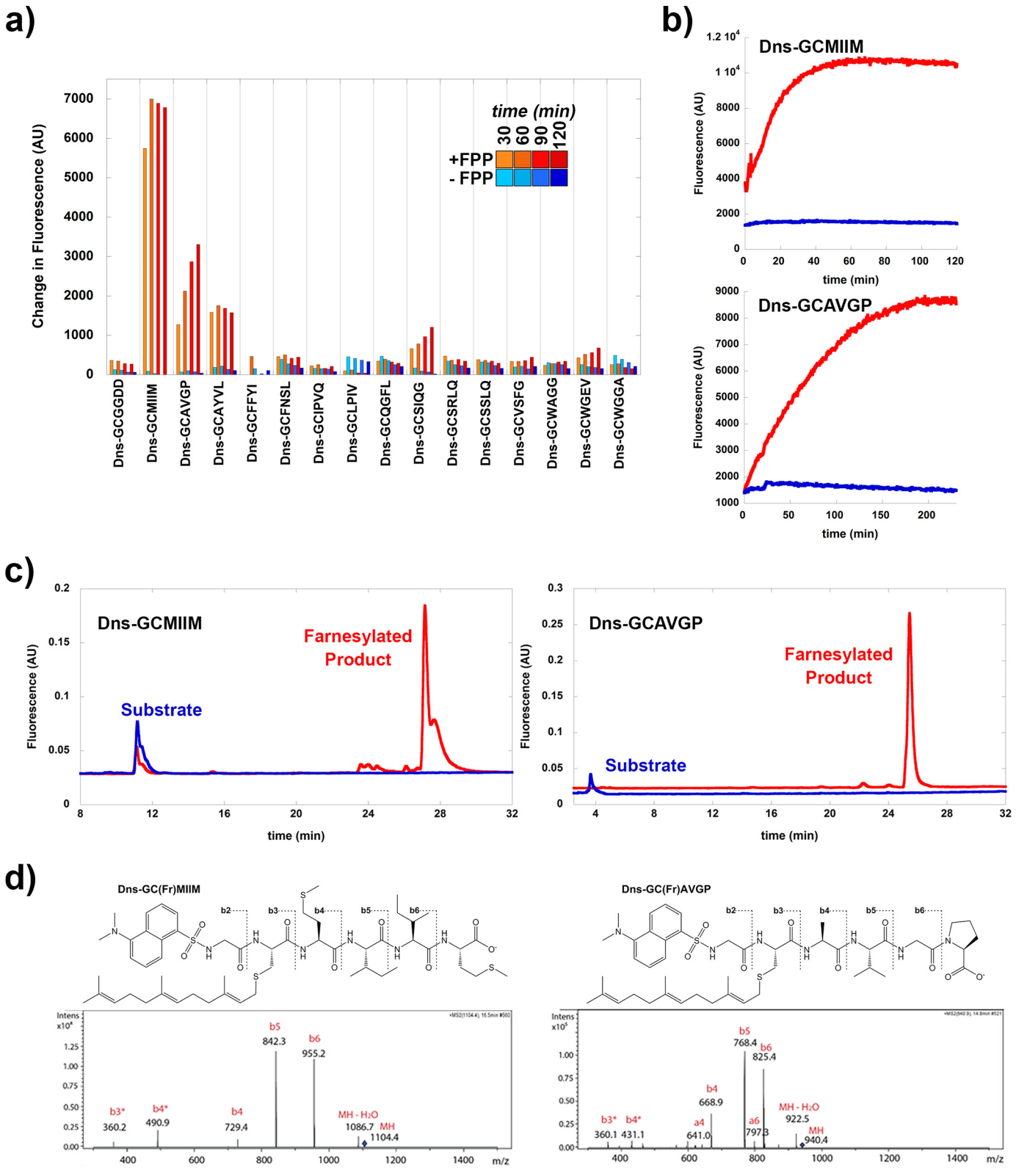

Figure 3. Dansyl-GC(*x*)$_3$*X* peptides can be efficiently farnesylated by mammalian FTase. *a,* fluorescence-based screening for FTase-catalyzed farnesylation of Dns-GC(*x*)$_3$*X* peptides. *b,* farnesylation of Dns-GCMIIM (*top*) and Dns-GCAVGP (*bottom*) by FTase as monitored by fluorescence enhancement reported in arbitrary units (*AU*). *Red trace,* farnesylation reaction; *blue trace,* control reaction lacking FPP. *c,* RP-HPLC analysis of FTase-catalyzed farnesylation of Dns-GCMIIM (*left*) and Dns-GCAVGP (*right*); substrate and farnesylated product peaks are labeled. *Red trace,* farnesylation reaction; *blue trace,* control reaction lacking FPP. *d,* ESI MS/MS analysis of farnesylated Dns-GCMIIM (*left*) and Dns-GCAVGP (*right*); *C*(*Fr*) indicates farnesylated cysteine. Reactions were performed and analyzed as described under "Experimental procedures"; tables of fluorescence screening data and ESI MS/MS ion assignments are included in the supporting data.

Table 2

Steady-state kinetic parameters for peptide reactivity with mammalian FTase and GGTase-I

Steady-state parameters were determined at saturating FPP (10 μM) or GGPP (10 μM) concentrations and varying peptide concentrations under conditions described under "Experimental procedures." Errors represent the standard deviation from a minimum of three replicates.

	Reactivity with FTase			Reactivity with GGTase-I		
	k_{cat}	K_m	k_{cat}/K_m	k_{cat}	K_m	k_{cat}/K_m
	s^{-1}	μM	$M^{-1}\,s^{-1}$	s^{-1}	μM	$M^{-1}\,s^{-1}$
Dns-GCVLS[a]	0.3	1.5	2×10^5	Not reported	Not reported	Not reported
Dns-GCAVGP	0.009 ± 0.001	5.6 ± 1.0	$1.6 \pm 0.3 \times 10^3$	No activity	No activity	No activity
Dns-GCAVG	0.14 ± 0.01	3.5 ± 0.3	$4.0 \pm 0.2 \times 10^4$	No activity	No activity	No activity
Dns-GCMIIM	0.009 ± 0.001	0.5 ± 0.1	$1.9 \pm 0.6 \times 10^4$	No activity	No activity	No activity
Dns-GCMII	0.040 ± 0.002	4.6 ± 0.6	$8.6 \pm 0.6 \times 10^3$	0.0070 ± 0.0003	0.50 ± 0.07	$1.4 \pm 0.1 \times 10^4$

[a] Data are from Ref. 64.

Dns-GC*AAX* peptides do not exhibit fluorescence enhancement upon prenylation (16), it appears the majority of the longer Dns-GC(*x*)$_3$*X* peptides examined are not compatible with the fluorescence-based assay. These false negatives in the FTase/FPP assay highlighted the importance of confirming the lack of Dns-GC(*x*)$_3$*X* peptide reactivity with GGTase-I by RP-HPLC. In contrast to FTase, none of the Dns-GC(*x*)$_3$*X* sequences were modified by GGTase-I when monitored by RP-HPLC, indicating that the C(*x*)$_3$*X* motif appears to be an FTase-specific target sequence.

Steady-state analysis of Dns-GC(x)$_3$X peptide reactivity with FTase and susceptibility to FTase inhibitor treatment

Steady-state kinetic analysis of the two peptides exhibiting the largest fluorescence enhancement upon prenylation, Dns-GCMIIM and Dns-GCAVGP, allows comparison of Dns-GC(*x*)$_3$*X* reactivity to peptides with canonical C*AAX* sequences such as Dns-GCVLS derived from H-Ras (65). The Dns-GCMIIM and Dns-GCAVGP peptides exhibit similar values for k_{cat}, with the K_m value for Dns-GCMIIM ~10-fold lower than that for Dns-GCAVGP (Table 2 and Fig. S1). Compared with Dns-GCVLS (k_{cat} = 0.3 s^{-1}, K_m = 1.5 μM) (65), k_{cat} values for both Dns-GC(*x*)$_3$*X* peptides are reduced ~30-fold, whereas K_m increases ~4-fold for Dns-GCAVGP and decreases ~3-fold for Dns-GCMIIM. When compared with Dns-GCMII and Dns-GCAVG, the potential sequences derived from proteolytic trimming, k_{cat}/K_m was increased 25-fold for Dns-GCAVG relative to Dns-GCVAGP and decreased 2-fold for Dns-GCMII relative to Dns-GCMIIM. These changes arise from changes in both k_{cat} (Dns-GCAVG) and K_m (Dns-GCMII), indicating the last residue of the C(*x*)$_3$*X* can impact both binding to FTase and substrate turnover. Among these four peptides, only Dns-GCMII serves as a GGTase-I substrate with a k_{cat}/K_m value comparable with Dns-GCMIIM with FTase ($1.4 \pm 0.1 \times 10^4$ M^{-1} s^{-1}, Table 2).

We next determined the effect of tipifarnib, a farnesyltransferase inhibitor, on the farnesylation of these peptide substrates (66, 67). Tipifarnib interacts with the peptide substrate-binding site within FTase (68). Treatment with tipifarnib efficiently blocked FTase-catalyzed farnesylation of Dns-GCMIIM (IC_{50} = 23 ± 7 nM) and Dns-GCAVGP (IC_{50} = 41 ± 13 nM) (Fig. S3). Tipifarnib inhibition of C(*x*)$_3$*X* peptide farnesylation suggests that these non-canonical sequences utilize many of the same interactions involved in C*AAX* peptide binding within the FTase active site.

eGFP-C(x)$_3$X reporter protein serves as an FTase substrate

To address the relevance of our findings in the context of larger substrates, we next explored the ability of a C(*x*)$_3$*X* sequence to be modified by FTase in the more biologically relevant context at the C terminus of a folded protein. We appended the reactive CAVGP sequence to the C terminus of eGFP, purified the bacterially expressed protein, and evaluated the farnesylation potential of the reporter using an approach validated for detecting modification of eGFP fusion proteins bearing canonical C*AAX* sequences (69, 70). Farnesylation of this eGFP-CAVGP reporter protein was assessed via LC-MS (Fig. 4). Following incubation in a reaction lacking the FPP co-substrate, only the unmodified eGFP-CAVGP protein is detected with a mass consistent with the expected unmodified protein (28205.1 Da). Upon incubation with both FTase and FPP, a new peak is detected in the chromatogram at a longer retention time with a mass of 28408.6 Da. This increased mass is the equivalent of eGFP-GCAVGP with the addition of a 204-Da (theoretical mass) farnesyl group, providing evidence of successful farnesylation of a full-length protein terminating in a C(*x*)$_3$*X* motif.

To further confirm FTase-catalyzed farnesylation of eGFP-CAVGP under *in vitro* conditions, we evaluated the ability of purified FTase to modify eGFP-CAVGP using an FPP analog (C15AlkOPP) bearing an alkyne group to allow for post-prenylation protein labeling. Following eGFP-CAVGP incubation with C15AlkOPP in the presence of FTase, the modified protein was derivatized with TAMRA-N_3 using Cu(II)-catalyzed alkyne-azide cycloaddition (CuAAC) (71, 72). In-gel imaging of TAMRA fluorescence revealed a single band at the expected size of farnesylated eGFP-GCAVGP (~28 kDa, Fig. 4*c*). The negative control reaction lacking the alkyne FPP analog does not exhibit a TAMRA-fluorescent band, with Coomassie Blue staining confirming the presence of eGFP-CAVGP in both reactions. Together, these results provide additional evidence for the farnesylation of a C(*x*)$_3$*X* motif by purified FTase in the context of a full-length protein.

Selection and reactivity analysis of C(x)$_3$X sequences derived from the human proteome

To address the relevance of our findings outside of yeast, we expanded our investigation to include C(*x*)$_3$*X* sequences derived from the human proteome to explore the potential biological relevance of this novel FTase substrate class. A scan of the Prosite database yielded 965 proteins in the human genome

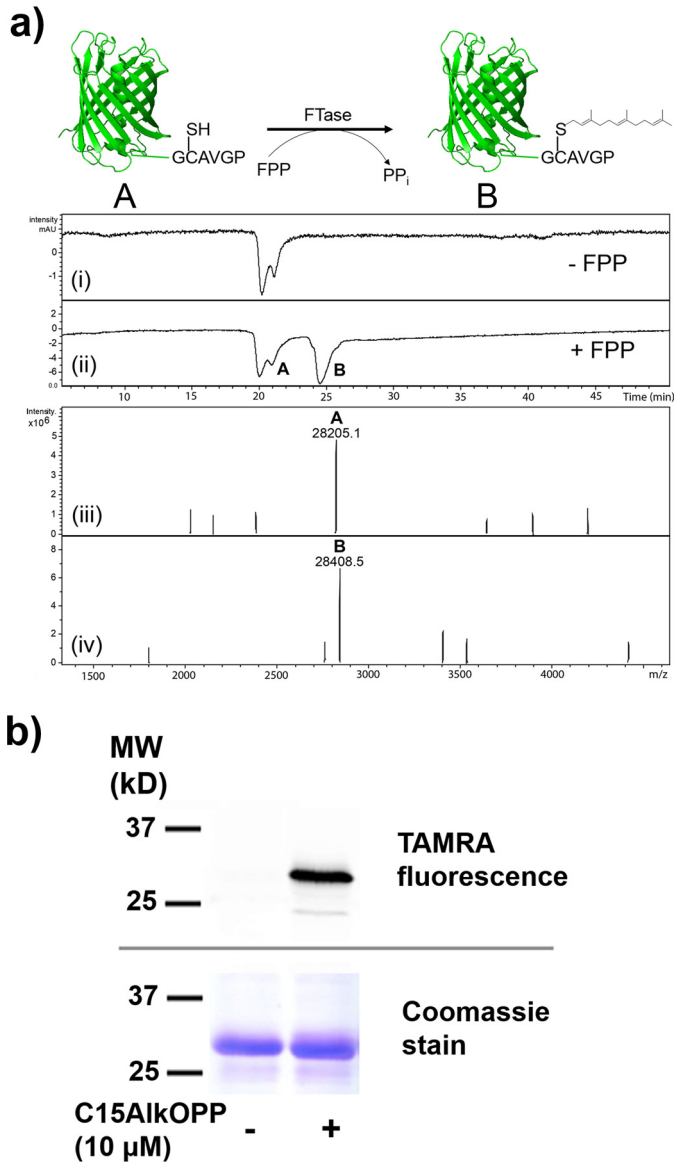

Figure 4. C(*x*)$_3$*X* sequence is efficiently farnesylated in the context of a protein substrate. *a,* LC-MS analysis of farnesylation of an eGFP reporter protein terminating in a C(*x*)$_3$*X* sequence. LC chromatogram of *in vitro* farnesylation of eGFP-GCAVGP using purified FTase in the absence (*panel i*) or presence (*panel ii*) of FPP, with absorbance detected at 555 nm. Negative absorbances are observed due to background fluorescence from eGFP. *Peaks A* (*panel iii*) and *B* (*panel iv*) have deconvoluted masses of 28,205.1 and 28,408.6 Da, respectively, that differ by 203.5 Da approximately corresponding to farnesyl modification (theoretical mass of farnesyl group: 204 Da). *b*, in-gel fluorescence scan (*top*) and Coomassie staining (*bottom*) of eGFP-GCAVGP subjected to *in vitro* prenylation using purified FTase in the presence or absence of C15AlkOPP.

containing a C(*x*)$_3$*X* C-terminal sequences. Of these proteins, six candidate sequences were selected for further characterization based on comparison with highly active sequences from the yeast studies (see "Experimental procedures"). Of the six human C(*x*)$_3$*X* sequences selected for analysis, three served as FTase substrates (Table 3). The two sequences resembling CAVGP, Dns-GCQTGP and Dns-GCSQGP, exhibited complete substrate farnesylation as determined by RP-HPLC, with the farnesylated peptide product of Dns-GCFSKM modification by FTase also detected (Fig. S2). None of the human-derived C(*x*)$_3$*X* peptides found to be substrates for FTase by RP-HPLC analysis exhibited sufficient fluorescence enhancement to allow steady-state characterization of peptide reactivity, underscoring that many C(*x*)$_3$*X* peptides appear refractory to detection of prenylation by fluorescence enhancement. As observed for the yeast C(*x*)$_3$*X* sequences, none of the human C(*x*)$_3$*X* sequences were substrates for rat GGTase-I when examined by either fluorescence enhancement or RP-HPLC (data not shown).

Fluorescence localization and metabolic labeling studies indicate a C(x)$_3$X sequence can support protein farnesylation in mammalian cells

To be considered biologically relevant FTase substrates, proteins terminating in C(*x*)$_3$*X* sequences must exhibit sufficient intrinsic reactivity to be modified by endogenous FTase within an intact cell. The minimum reactivity for human substrates is estimated to be in the range of $k_{cat}/K_m = 0.5–2 \times 10^4\ M^{-1}\ s^{-1}$ when peptide substrate reactivity is ascertained in an *in vitro* assay using purified FTase (73). The reactivity of the Dns-GCMIIM peptide with purified FTase ($k_{cat}/K_m = 1.9 \pm 0.6 \times 10^4\ M^{-1}\ s^{-1}$, Table 2) suggests that the CMIIM sequence is sufficiently reactive to support protein farnesylation within mammalian cells. The apparent reactivity observed for this sequence within yeast cells further suggests the ability of this motif to be modified in a cellular setting.

To examine CMIIM reactivity within a mammalian cellular context, this sequence was introduced into a previously described fusion protein consisting of eGFP fused to the C-terminal domain of K-Ras4B. This reporter displays membrane localization upon prenylation of its canonical C-terminal CVIM sequence (74). Following transient transfection into HEK293 cells, eGFP-KRas-CMIIM also displayed membrane-localized fluorescence consistent with its farnesylation (Fig. 5). Treatment with tipifarnib during transfection leads to diffuse eGFP-KRas-CMIIM fluorescence, as does mutation of the C(*x*)$_3$*X* cysteine to a serine (eGFP-KRas-SMIIM). A reporter protein lacking the last residue of the CMIIM sequence (eGFP-KRas-CMII) was also examined to determine whether localization of C(*x*)$_3$*X* proteins was due to endogenous proteolysis. eGFP-KRas-CMII also displays membrane-localized fluorescence but is unaffected by tipifarnib treatment. This behavior is consistent with the reactivity of the CMII sequence with GGTase-I (Table 2), which would lead to prenylation and membrane localization in the presence of tipifarnib. This result also underscores the FTase selectivity of the CMIIM sequence and further demonstrates that proteolytic trimming of the sequence does not occur within the cell.

To directly confirm prenylation of the eGFP-KRas-CMIIM reporter protein by endogenous FTase within a mammalian cell, we employed metabolic labeling of transiently transfected HEK293 cells using an alkyne-containing FPP analog (75). Following transient transfection with eGFP-KRas-derived fusion proteins, cells were incubated with the C15AlkOPP FPP analog for alkyne functionalization of the expressed protein. Cell lysates were derivatized with TAMRA-N_3 as described above. Transfection with eGFP-KRas-CVIM as a positive control followed by in-gel imaging of TAMRA fluorescence resulted in a single major band at the expected size of this fusion protein

Table 3
Mammalian FTase reactivity with C(*x*)$_3$*X* sequences derived from the human genome

Peptide	Human protein	HPLC detection of farnesylated Dns-GC(x_3)*X*
Dns-GCLLHP	Ras association domain-containing protein 5	−
Dns-GCSQGP	Sushi, nidogen and EGF-like domain-containing protein 1	+
Dns-GCQTGP	Putative glycosylation-dependent cell adhesion molecule 1	+
Dns-GCSVKM	Olfactory receptor protein	−
Dns-GCFSKM	Sorting nexin 4	+
Dns-GCDREV	Prostamide/prostaglandin F synthase	−

(~50 kDa), with this band not observed in untransfected cells or transfected cells not treated with the C15AlkOPP analog (Fig. 5*c*). A similar predominant TAMRA-fluorescent band was observed at the expected size of eGFP-KRas-CMIIM in the presence of C15AlkOPP. This single predominant band was not observed when the CMIIM sequence in the reporter was mutated to SMIIM, with the SMIIM sample resembling the untransfected cell negative control. The loss of reporter protein detection with the SMIIM sequence would be expected due to the lack of a cysteine at the farnesylation site.

To provide further evidence that the eGFP-KRas-CMIIM protein is farnesylated *in vivo*, the alkyne-modified protein can be enriched because of the presence of the appended alkyne isoprenoid analog that is amenable to conjugation with an affinity handle. Thus, a quantitative chemical proteomic analysis was performed on lysates obtained from eGFP-KRas-CMIIM-transfected *versus* eGFP-KRas-SMIIM-transfected cells grown in the presence of C15AlkOPP. Lysates were biotinylated with biotin-N_3 followed by pulldown with avidin resin. Enriched proteins were digested, labeled with a tandem mass tag (TMT), and analyzed via LC-MS/MS. A volcano plot generated after performing a two-sample *t* test (FDR = 0.05, s0 = 0.5) across three replicates strongly indicates that eGFP-KRas-CMIIM is enriched over eGFP-KRas-SMIIM, further evidencing the *in vivo* farnesylation of this protein (Fig. 5*d*). Parallel gel-based studies of eGFP-KRas reporter proteins terminating in other FTase-reactive C(*x*)$_3$*X* sequences failed to demonstrate metabolic labeling within transfected cells. This may reflect that the lower reactivity of these sequences (*e.g.* CAVGP is 10-fold less reactive than CMIIM, Table 2) is insufficient to support direct detection of transfected protein prenylation within cells by metabolic labeling or imaging methods (73). Nevertheless, these imaging, metabolic labeling, and quantitative proteomic studies support FTase-catalyzed lipidation of eGFP-KRas-CMIIM within the cell, indicating that a C(*x*)$_3$*X* sequence can be sufficiently reactive to support biologically relevant protein farnesylation.

Discussion

Protein prenylation by FTase and GGTase-I is an important modification occurring on many targets within the proteome. Following more than 2 decades of biochemical, structural, and computational investigation of these enzymes and their protein substrates, a C-terminal C*AAX* sequence has been defined as the signature recognition motif for both FTase and GGTase-I. In this work, we have identified multiple C-terminal C(*x*)$_3$*X* sequences representing a new class of substrates for FTase. These unanticipated substrates broaden the range of FTase substrate selectivity and expand the array of potential prenylation targets well beyond that predicted by previous biochemical, structural, and computational studies. Our findings provide the foundation for continuing studies toward identifying physiologically relevant C(*x*)$_3$*X* proteins within the proteome. This new substrate class carries with it the potential to expand the involvement of prenylated proteins within biology, with associated implications ranging across the biochemical, cell biology, and biomedical communities.

The ability of FTase to prenylate C(*x*)$_3$*X* sequences was not predicted based on the current understanding of FTase recognition of C*AAX* sequence substrates. Multiple structural studies of FTase and GGTase-I complexes with peptide substrates supported substrate length selectivity defined by two contact points: 1) the distance between the coordination of the cysteine of the C*AAX* sequence to the catalytic zinc ion, and 2) multiple hydrogen bonds (both direct and water-mediated) between the C-terminal carboxylate of the C*AAX* sequence and residues in both subunits of FTase or GGTase-I (45, 76–78). Several of these interactions serve as constraints in the FlexPepBind approach for predicting peptide sequence reactivity with FTase. When applied to selected FTase-reactive C(*x*)$_3$*X* sequences, FlexPepBind only predicts ~50% of the HPLC-verified FTase substrates (Table S4) (46). The ability of FTase to accept the longer C(*x*)$_3$*X* motif indicates that its active site is more flexible than previously proposed. In contrast, the inability of GGTase-I to accept these C(*x*)$_3$*X* substrates shows that it exhibits distinct length and/or sequence requirements, adding to the functional distinctions between these two closely related enzymes. We expect in future studies to define the sequence selectivity within the C(*x*)$_3$*X* sequence and to explore the effect of changing the prenyl donor cosubstrate on C(*x*)$_3$*X* substrate reactivity, for comparison with prenyl–donor-dependent changes in peptide substrate selectivity seen with C*AAX* substrates (54, 79). These studies will provide functional insight into the interactions formed with these longer peptide sequences within the FTase active site. Understanding the active-site adjustments required for FTase recognition and modification of C(*x*)$_3$*X* sequences will be aided by structural and computational modeling studies of peptides from this new substrate class in complex with FTase.

The ability of both mammalian and yeast FTase to farnesylate proteins with the longer C(*x*)$_3$*X* motif has the potential to greatly expand the number of potential FTase substrates within the human and yeast proteomes. The human proteome is predicted to contain 965 proteins terminating in C(*x*)$_3$*X* sequences, with 773 of these sequences containing only a single cysteine residue. This representation nearly matches that of C*AAX* sequences in the human proteome (1166 sequences; 1021 with a single cysteine). Biochemical and computational studies indi-

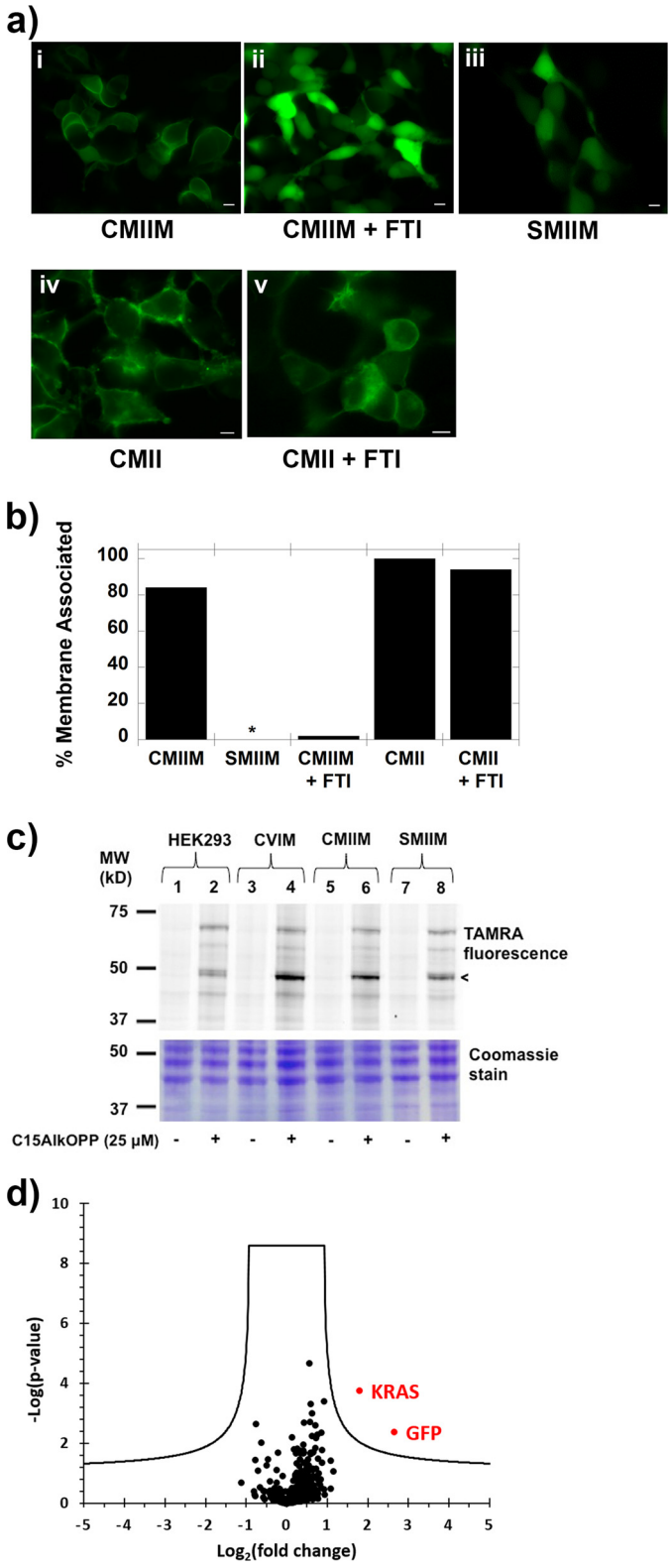

Figure 5. eGFP-KRas-CMIIM is efficiently modified by FTase within a mammalian cell. *a,* representative images of HEK293 cells transfected with eGFP-KRas-XMIIM or eGFP-KRas-CMII reporter proteins in the absence or presence of tipifarnib (*FTI*); *scale bar,* 20 μm. *b,* scoring of fluorescence patterns observed in HEK293 cells after transfection with eGFP-KRas reporter proteins; an *asterisk* indicates no cells exhibited membrane-associated fluorescence. Detailed scoring data are provided in Table S3. *c,* in-gel fluorescence scan (*top*) and Coomassie staining (*bottom*) of lysates from HEK293 cells transfected with eGFP-KRas reporter proteins and metabolically labeled with C15AlkOPP followed by conjugation of a TAMRA-N_3 fluorophore. Cells were either non-transfected (HEK293) or transfected with eGFP-KRas-CVIM, eGFP-KRas-CMIIM, or eGFP-KRas-SMIIM reporter proteins in the absence or presence of C15AlkOPP. *d, volcano plot* for TMT-labeled quantitative proteomic analysis of eGFP-KRas-CMIIM- *versus* eGFP-KRas-SMIIM-transfected HEK293 cells treated with C15AlkOPP and enriched via biotin-avidin pulldown. A two-sample *t* test (FDR = 0.05, s0 = 0.5) from three replicates shows that GFP and KRas are statistically enriched in eGFP-KRas-CMIIM transfected cells.

cate that a large fraction of these *CAAX* sequences can serve as FTase substrates, raising the possibility that a large fraction of C(*x*)$_3$*X* sequences could also be farnesylated (16, 46). Although fewer in number, a similar proportion of proteins bearing C(*x*)$_3$*X* and *CAAX* motifs is observed in the *Saccharomyces cerevisiae* proteome with 117 C(*x*)$_3$*X* proteins (88 with a single cysteine) and 120 *CAAX* proteins (101 with a single cysteine). Although this study verified farnesylation of human protein-derived C(*x*)$_3$*X* sequences in the context of small peptide substrates, inclusion of C(*x*)$_3$*X* proteins doubles the potential scope of prenylation within the human and yeast proteomes. Similar expansions of potentially farnesylated proteins could be expected in pathogenic organisms that employ either endogenous or host-mediated farnesylation, such as *Plasmodium falciparum, Candida albicans,* and *Legionella pneumophila* (75, 80–85). Our expansion of the potential substrates recognized by FTase, supported by the reactivity of human-derived C(*x*)$_3$*X* peptide sequences, highlights the importance of continuing studies toward identifying additional new and biologically relevant protein substrates and determining their prenylation state within the cell. In particular, identification and isolation of endogenously prenylated C(*x*)$_3$*X* proteins will be essential for understanding the biological impact of prenylation of non-canonical FTase substrates. These cellular studies will be greatly aided by the demonstrated ability of metabolic labeling to bioorthogonally functionalize a prenylated C(*x*)$_3$*X* protein. A key challenge in this work will be determining the minimum level of substrate protein reactivity required for efficient metabolic labeling. Defining this parameter will provide valuable insight into the applicability of this technique for identifying biologically relevant targets. Given the established involvement of prenylation in a range of disease states, our findings also carry the potential to establish a link between farnesylation of unanticipated protein targets and cellular dysfunction that could be exploited for treatment with the available range of potent farnesyltransferase inhibitors.

In addition to expanding the scope of prenylation within the proteome, our findings further support the "shunt pathway" model for protein prenylation wherein a subset of farnesylated proteins can sidestep subsequent C-terminal processing steps (32). Such proteins with canonical *CAAX* motifs include Ydj1p, Rab38, Phkα/β, and Gγ5 (27, 32, 86, 87). The majority of C(*x*)$_3$*X* sequences described in this study were identified in yeast using a Ydj1p-based screen that discriminates for shunted sequences. Although none of the Ydj1p screen-derived C(*x*)$_3$*X* sequences are present in either the yeast or human proteomes, similar sequences do exist and are reactive for farnesylation as demonstrated by the human sequences examined in this work. Our findings inspire several important questions. First, how many naturally occurring C(*x*)$_3$*X* proteins are prenylated? Second, what fraction of naturally occurring prenylated C(*x*)$_3$*X* proteins

are refractory to subsequent processing (*i.e.* shunted)? Third, how does subsequent processing, or lack thereof, affect the biological properties of prenylated C(*x*)$_3$*X* proteins? Identifying novel protein prenyltransferase C(*x*)$_3$*X* protein substrates may require application of chemical biology proteomics-based approaches or development of new analytical tools for detecting endogenously prenylated proteins, especially because traditional assays for detecting *in vivo* prenylation (*e.g.* membrane localization) may not be relevant to shunted proteins whether they are of the C*AAX* or C(*x*)$_3$*X* variety.

Experimental procedures

Miscellaneous methods

All *in vitro* FTase and GGTase-I assays were performed at 25 °C. All curve fitting was performed with KaleidaGraph (Synergy Software, Reading, PA). Geranylgeranyl diphosphate (GGPP) and farnesyl diphosphate (FPP) were purchased from Isoprenoids.com (Tampa, FL). Peptides were commercially synthesized (Sigma Genosys) and exhibited >90% purity, as determined by RP-HPLC or after semi-preparative purification via RP-HPLC. Peptides were solubilized in ethanol containing 10% (v/v) DMSO and stored at −20 °C. Peptide concentrations were determined spectrophotometrically using Ellman's reagent (88). The isoprenoid analog C15Alk-OPP was prepared as described previously (64).

Yeast strains and plasmids

The yeast strains used in this study were IH1793 (*MATα lys1*), RC757 (*MATα sst2-1 rme his6 met1 can1 cyh2*), SM2331 (*MAT***a** *trp1 leu2 ura3 his4 can1 mfa1 mfa2*), yWS304 (*MAT***a** *his3Δ1 leu2Δ0 met15Δ0 ura3Δ0 ydj1::KAN*^{R}), and yWS1632 (*MAT***a** *his3Δ1 leu2Δ0 met15Δ0 ura3Δ0 ram1::KAN*^{R}) and have been previously described (32, 57, 89, 90). These strains were routinely propagated at 30 °C (IH1793, RC757, and SM2331) or room temperature (yW304 and yWS1632) on either YPD or appropriate selective media when plasmid-transformed. pRS315 (*CEN LEU2*), pSM1605 (*2μ URA3 MFA1*), pWS610 (*CEN LEU2 MFA1*), pWS612 (*CEN LEU2 MFA1-CASQ*), pWS942 (*CEN URA3 YDJ1*), pWS1132 (*CEN URA3 YDJ1-SASQ*), pWS1246 (*CEN URA3 YDJ1-CTLM*), and pWS1286 (*CEN URA3 YDJ1-CVIA*) have been previously described (32, 91–93).

pWS705 (*2μ URA3 MFA1-CGGDD*), pWS1170 (*CEN URA3 YDJ1-CVLMM*), pWS1488 (*CEN URA3 YDJ1-CMIIM*), pWS1111 (*CEN LEU2 MFA1-CMIIM*), and pWS1112 (*CEN LEU2 MFA1-CVLMM*) were constructed by PCR-directed, recombination-mediated plasmid construction (94). In brief, PCR products designed to amplify the 3′-ends of *MFA1* and *YDJ1* with encoding for the desired C(*x*)$_3$*X* motifs were used to gap repair plasmids pSM1605 (*2μ URA3 MFA1*), pWS1024 (*CEN URA3 MFA1-C*IA*; where* indicates a premature TAG stop codon at the a_1 position of C*AAX* motif; this plasmid was created by recombination-based methods from pWS610 and pWS1132 (*CEN URA3 YDJ1-SASQ*), as described previously (32, 92). These plasmids and others identified through our screening methods were introduced into strains via a lithium acetate-based transformation procedure (95).

Oligonucleotide design for generation of randomized C(x)$_3$X sequences by PCR

Synthetic oligonucleotides were designed to PCR-amplify the C*AAX* encoding region and associated 3′-untranslated region of either *MFA1* or *YDJ1* as encoded in pWS1024 and pWS1132, respectively. The forward PCR oligo was designed to encode the C(*x*)$_3$*X* sequences and was flanked on the 5′-end by 39 nucleotides homologous to the appropriate gene immediately before the C*AAX* motif (to facilitate recombination) and on the 3′-end by a stop codon and additional nucleotides homologous to the 3′-untranslated region (to facilitate PCR priming). The oligo used for generation of CGGDD was designed to encode these specific amino acids. The oligo used to generate a library of C(*x*)$_3$*X* sequences was synthesized to encode a cysteine codon followed by four random codons and a stop codon. To limit the complexity of the codons synthesized yet allow for all possible amino acids, only C, G, and T were used at the wobble position of the $(x)_3$ codons. To prevent formation of a premature stop codon yielding a canonical length motif (i.e. CXXX) that would lead to false positives, only A, C, and G were used at the first position of the X codon; this strategy unfortunately disallowed incorporation of Cys, Phe, Trp, and Tyr codons.

a-factor–mating pheromone screen, halo assay, and mating test

SM2331 yeast was cotransformed with MluI- and SphI-digested pWS1024 and PCR products engineered to encode 5-mer sequences. The transformation mix was plated on SC-leucine solid media and incubated at 30 °C for 72–96 h. Estimates of colony numbers were determined, and then colonies were replica-plated onto a fresh SC-leucine plate as well as a YPD plate containing a thin lawn of RC757 yeast prepared in the presence of 0.071% Triton X-100 (final concentration in cell suspension prior to lawn preparation), and plates were incubated at 30 °C for 16–20 h. Colonies displaying a halo were identified, and the corresponding colony on the SC-leucine replicate plate was recovered. Expression of **a**-factor was confirmed by amplifying selected colonies in SC-leucine liquid media and applying 20× concentrated spots of liquid culture onto RC757 lawns in the presence and absence of Triton X-100. Plasmids were isolated and sequenced from the strongest halo producing strains.

A modified version of the halo assay was used to assess relative strength of **a**-factor production by the various **a**-factor C*AAX* mutants evaluated. Plasmid-transformed *MAT***a** strains were cultured in appropriate selective media (SC-leucine or SC-uracil), spotted onto YPD, and incubated for 24–36 h at 30 °C. The spots on the plate were replica-transferred onto a thin lawn RC757 yeast (no Triton X-100), and plates were incubated at 30 °C for 16–20 h.

The quantitative mating test was performed essentially as described previously (32). In brief, the *MAT***a** strains were independently cultured to saturation in selective media, and the IH1793 *MATα lys1* strain was cultured in YPD. All strains were diluted to A_{600} ~1.0 using fresh culture media. Empirically determined dilutions were spread on SD and SC-lysine solid

media; the former media is diploid-selective, and the latter is selective for *MAT***a** haploid cells and *MAT***a** cells that have undergone mating to form a diploid cell. The total count of colony-forming units (CFUs) on each media type was determined and used to calculate a mating frequency (*i.e.* diploid CFUs over total CFUs); this value was used to determine the percentage mating of each condition relative to the strain producing wildtype **a**-factor.

Thermotolerance screen

yWS304 yeast was co-transformed with NheI-digested pWS1132 and the PCR product engineered to encode randomized 5-mer sequences. A percentage of the transformation mix was plated on SC-uracil solid media and incubated at 25 °C for 96 h to assess the total number of colonies, indicative of the number of plasmids created by the transformation procedure. The remaining transformation mix was plated on YPD solid media and incubated at 40 °C for 96 h. Colonies recovered by high temperature selection were re-tested for thermotolerance as patches on YPD, and individual plasmids were recovered and sequenced. The isolated plasmids were re-introduced into yWS304 to confirm plasmid-linked thermotolerance prior to detailed thermotolerance analysis.

Thermotolerance assay

Saturated cultures grown in SC-uracil liquid media at room temperature were serially diluted into YPD and spotted onto YPD solid media (5 μl per spot), as described previously (32). Plates were incubated at various temperatures (25, 37, or 40 °C) for several days before plate imaging. Each experiment was performed at least twice on separate days, and each strain was evaluated in duplicate within each experiment.

Estimate of C(x)$_3$X complexity in a-factor and thermotolerance screens

The estimated coverage of C(x)$_3$$X$ sequences evaluated was calculated using the GLUE-IT algorithm based on the number of colonies screened and the number and redundancy of the codons used for amino acid randomization (58). The number of colonies screened with the **a**-factor reporter was determined by direct colony counts on all plates evaluated. The number of colonies screened with the Ydj1p reporter was estimated from the colony numbers observed for the percentage of the transformation mix plated onto selective media at a non-selective temperature. The number of false-positive colonies was not counted toward the total number of colony-forming units; the false-positive numbers were determined from transformation mixtures containing the linearized plasmids and PCR products alone that typically yielded a smaller number of CFUs relative to a cotransformed sample (total typically $<$2%).

Immunoblot analysis for protein prenylation in yeast

Whole-cell lysates of mid-log yeast were prepared as described previously using alkaline hydrolysis and TCA precipitation (32, 96). Samples and PageRuler size standards (Thermo Fisher Scientific, Waltham, MA) were separated by SDS-PAGE (12.5%), transferred onto nitrocellulose, and the blots incubated with rabbit anti-Ydj1p primary antibody (courtesy of Dr. Avrom Caplan) and HRP-conjugated donkey anti-rabbit secondary antibody (GE Healthcare). Immune complexes were detected by X-ray film after treatment of blot with HyGLO development solution (Denville Scientific, South Plainfield, NJ).

Image analysis for yeast assays and immunoblots

Plates and developed films were imaged using a flat-bed scanner (300 dpi; grayscale), and resultant TIFF image files were manipulated with Photoshop (*i.e.* image rotation, image contrast adjustments, and cropping) before final figure assembly using PowerPoint. Plates were scanned face down without lids using a black background. Films were scanned using a white background. For all plate scans, contrast settings were adjusted manually using the same settings for all images. For film scans, contrast settings were adjusted using Photoshop's "Auto Contrast" function.

Activity screening of Dns-GC(x)$_3$X peptides by fluorescence-based prenylation assay

Prenylation of dansylated Dns-GC(x)$_3$$X$ peptides was assessed by a time-dependent increase in fluorescence (λ_{ex} 340 nm, λ_{em} 520 nm) upon prenylation of the dansylated peptide (16, 44, 60–62). Assays were performed at 25 °C in a 96-well plate (Corning, Corning, NY). Fluorescence was measured as a function of time in a Synergy H1 multimode plate reader (Biotek, Winooski, VT). Negative controls lacked the FPP or GGPP cosubstrate.

To assess the reactivity of Dns-GC(x)$_3$$X$ peptides with FTase and GGTase-I, time-course reactions were performed in the presence and absence of FPP and GPP. Fluorescence was measured for each peptide at time 0 (F_0) and four time points (F_t; t = 30, 60, 90, and 120 min). Corrected fluorescence ($F_t - F_0$) values were calculated for each time point and condition (Table S1). To be considered reactive, a peptide must exhibit at least a 5-fold enhancement of fluorescence in the FTase or GGTase-I reaction compared with the negative control (*e.g.* corrected fluorescence (+FPP)/corrected fluorescence (−FPP) $>$ 5). None of the Dns-GC(x)$_3$$X$ peptides exhibited fluorescence enhancement in reactions with GGTase-I and GGPP.

Activity screening prenylation of Dns-GC(x)$_3$X peptides via RP-HPLC

RP-HPLC analysis was performed on all Dns-GC(x)$_3$$X$ peptides to confirm farnesylation (FPP and FTase) or geranylgeranylation (GGPP and GGTase-I). Reactions were prepared as described above for fluorescence-based activity screening and incubated at room temperature for 14 h in low-adhesion tubes wrapped in foil. Reactions were halted by addition of an equal volume of 20% acetic acid in isopropyl alcohol prior to analysis by RP-HPLC (Zorbax Eclipse XDB-C18 column). Peptides and products were detected by fluorescence (λ_{ex} = 340 nm, λ_{em} = 496 nm). In all cases, the peak for the Dns-GC(x)$_3$$X$ peptide shifts to a longer retention time upon farnesylation, whereas parallel reactions performed without FPP showed no change in peptide retention time. Representative RP-HPLC traces are included as Fig. S2. Analogous reactions with GGTase-I and

GGPP provided no evidence for geranylgeranylation of Dns-GC(x)$_3X$ peptides.

Steady-state characterization of Dns-GC(x)$_3$X and Dns-GCAAX peptides

Steady-state kinetics were determined as described previously for prenylation of Dns-GC(x)$_3X$ and Dns-GC*AAX* peptides by FTase or GGTase-I by monitoring the time-dependent increase in fluorescence (λ_{ex} 340 nm, λ_{em} 520 nm) upon prenylation of the dansylated peptide in a Synergy HI multimode plate reader (Biotek) (43, 59, 63).

Determination of tipifarnib inhibition of Dns-GC(x)$_3$X peptide farnesylation

Assays were performed as described above for fluorescence-based detection of peptide farnesylation, with varying concentrations of tipifarnib (0–100 nM) included in the reaction. Initial slopes (fluorescence change per s) were determined for each reaction and normalized to the reaction without tipifarnib. Normalized slope values were plotted against tipifarnib concentration and analyzed using Equation 1 to calculate IC_{50} values.

$$\text{normalized slope} = 1 - \frac{[\text{tipifarnib}]}{[\text{tipifarnib}] + IC_{50}} \quad \text{(Eq. 1)}$$

ESI-MS analysis of farnesylated Dns-GC(x)$_3$X peptides

In vitro reactions with Dns-GC(x)$_3X$, peptides (5 μM) were prepared in prenylation buffer (50 mM NaHEPPSO, 5 mM TCEP, pH 7.8) in the presence of 100 nM FTase and 10 μM FPP and incubated overnight at room temperature. Each reaction mixture was separately loaded onto a pre-conditioned and pre-equilibrated Sep-Pak reverse-phase C18 cartridge (Waters Corp., Milford, MA) and washed with 0.1% TFA in H_2O. A step-gradient elution was carried out with 6-ml volumes of 10% (CH_3CN/H_2O; 0.1% TFA), 35% (CH_3CN/H_2O; 0.1% TFA), and 100% CH_3CN with 0.1% TFA. The 100% CH_3CN fractions containing the modified peptides (confirmed by fluorescence under UV lamp) were evaporated, and residues were redissolved in 30% CH_3CN/H_2O with 0.1% TFA. Samples were loaded onto an LC column (Zorbax SB-C18, 5 μm × 150 mm × 0.5 mm) coupled to an ESI-MS/MS ion trap mass analyzer (Agilent 1100 Series LC-MSD). Runs were set to positive ion mode, and collision-induced dissociation MS/MS fragmentations were triggered at 1.5 V. The theoretical masses of farnesylated peptides and their fragments were calculated using Protein Prospector version 5.19.1.

Construction of pJExpress414 plasmid encoding the His$_6$-eGFP-GCAVGP reporter protein

A gene encoding the His_6-eGFP-GCAVGP reporter protein was prepared by PCR using the pJExpress414-eGFP-CVIA vector as a template with the GCAVGP C-terminal sequence and HindIII restriction site encoded in the 3′-primer (97). PCR products were purified using the EZ-10 spin column PCR purification kit following the manufacturer's instructions, BioBasic Inc. (Amherst, NY). Following digestion by NheI and HindIII, the His_6-eGFP-GCAVGP insert was ligated into the pJExpress414 expression plasmid using the Quick Ligase kit (New England Biolabs, Ipswich, MA) per the manufacturer's instructions. Insert ligation was verified by analytical restriction digest and DNA sequencing (Genewiz, South Plainfield, NJ).

Expression and purification of His$_6$-eGFP-GCAVGP

Chemically competent BL21 (DE3) *Escherichia coli* (Z-competent, ZymoResearch, Irvine, CA) cells were transformed with pJExpress414_His_6-eGFP-GCAVGP per the manufacturer's protocol. Following transformation and antibiotic selection, a colony from the transformation plate was inoculated into LB media (5 ml) containing 100 μg/ml ampicillin. The culture was incubated with shaking (225 rpm) for 4 h at 37 °C and subsequently used to inoculate 1 liter of prewarmed autoinduction media supplemented with 100 μg/ml ampicillin (98). Following overnight incubation at 28 °C with shaking, bacteria were harvested, lysed, and His_6-eGFP-GCAVGP-purified as described previously (70). Protein concentration was measured using absorbance of eGFP at 488 nm (ϵ_{488} = 55,000 M^{-1} cm^{-1}) (99).

Farnesylation reactions with His$_6$-eGFP-GCAVGP

Farnesylation of purified His_6-eGFP-GCAVGP was performed by incubation of purified protein (5 μM) with 100 nM FTase, 10 μM FPP or C15AlkOPP, and 5 mM $MgCl_2$ in reaction buffer (50 mM NaHEPPSO, 5 mM TCEP, pH 7.8) in a final volume of 2 ml (FPP, mass spectrometry analysis) or 500 μl (C15AlkOPP, TAMRA-N_3 labeling and in-gel fluorescence analysis). Substrate protein was incubated in reaction buffer for 20 min prior to reaction initiation by addition of FTase and prenyl donor to reduce disulfide bonds. Reactions were incubated overnight at room temperature wrapped in foil and then frozen for storage. *In vitro* reaction mixtures were concentrated by lyophilization and injected to an LC column (Zorbax 300SB-C8, 3.5 μm × 100 mm × 0.3 mm) coupled to an ESI-MS/MS ion trap mass analyzer (Agilent 1100 Series LC-MSD). The proteins were eluted with buffer A (0.1% HCO_2H in H_2O) and buffer B (0.1% HCO_2H in CH_3CN) in the following gradient segments of buffer B: 2 min, 10%; 3 min, 10–25%; 35 min, 25–60%; 10 min, 60–90%. The m/z values from protein fragments were deconvoluted to estimate parent protein masses. Prior to in-gel fluorescence labeling, His_6-eGFP-GCAVGP from *in vitro* farnesylation reactions (±10 μM C15AlkOPP) was recovered using a protein precipitation kit (ProteoExtract, Calbiochem). Protein pellets were redissolved in PBS + 1% SDS, and 14 μg of proteins was subjected to click reaction (25 μM TAMRA-N_3, 1 mM TCEP, 0.1 mM TBTA, and 1 mM $CuSO_4$) for 1 h at room temperature. An aliquot (3.5 μg) from the click reactions were mixed with Laemmli loading buffer, boiled for 5 min, and analyzed using a 15% SDS-polyacrylamide gel. In-gel fluorescence was detected using a fluorescence scanner (Typhoon FLA 9500, GE Healthcare; λ_{ex} 542 nm, λ_{em} 568 nm). Gels were stained with Coomassie Blue and destained to visualize protein loading. Images were processed on ImageJ.

Identification of human C(x)$_3$X sequences

To identify human C(x)$_3X$ sequence candidates, we interrogated the Prosite database (http://prosite.expasy.org/

scanprosite/)[3] using highly active sequences from the yeast studies (CAVGP, CMIIM, and CWGEV) and allowing sequence variability at one, two, or three positions downstream of the cysteine residue. Sequences containing more than one cysteine were eliminated to avoid canonical four-amino acid *CAAX*-compliant motifs (example: CCIIM) or sequences potentially recognized by GGTase-II (examples: CC or C*X*C) (18, 20). The candidate sequences were chosen based on previous studies of the protein bearing the C(*x*)$_3$*X* sequences, their location within the cell (*e.g.* membrane associated), and the degree of sequence similarity to the parent C(*x*)$_3$*X* sequence from the yeast studies.

Construction of eGFP-KRas-C(x)$_3$X reporter protein plasmids

Gene inserts encoding eGFP-KRas-*X*MIIM (*X* = C or S) and eGFP-KRas-CMII reporter proteins were prepared by PCR using the pEGFP-KRas vector (Casey Lab, Duke University) as a template with the CMIIM, SMIIM, or CMII C-terminal sequences and KpnI restriction site encoded in the 3′-primers (100). PCR products were purified using the BioBasic Inc. EZ-10 spin column PCR purification kit following the manufacturer's instructions. Following digestion by NheI and KpnI, the eGFP-KRas-*X*MIIM or eGFP-KRas-XMII insert was ligated into the pEGFP-KRas expression plasmid using the Quick Ligase™ kit (New England Biolabs) per the manufacturer's instructions. Insert ligation was verified by analytical restriction digest and DNA sequencing (Genewiz, South Plainfield, NJ).

Cell culture, transfection, and imaging

HEK293 cells (ATCC) were maintained in 75-ml vented tissue culture flasks (Celltreat, Pepperell, MA) and were split upon reaching 80% confluency. Cells were grown in complete DMEM (DMEM supplemented with 10% fetal bovine serum and 1% (v/v) penicillin/streptomycin (MediaTech, Manassas, VA)) in 5% CO_2 at 37 °C. Transfections and imaging were performed, as described previously (73), in a single glass well imaging dish (Corning) and allowed to adhere for 24 h prior to addition of Turbofect transfection reagent (Thermo Fisher Scientific) according to the manufacturer's protocol. Tipifarnib was added to a final concentration of 10 nM to the transfection mixture for those cells undergoing inhibitor studies. Following 36 h of transfection, live cells were imaged at ×63 magnification using a Zeiss AxioVert.A1 inverted fluorescence microscope with a 470/40 nm excitation filter, a 495-nm beam splitter, and a 525/50-nm emission filter. Images were captured using a Zeiss Axiocam MRm camera and analyzed using Zen Pro software (Zeiss).

Metabolic labeling of HEK293 cells expressing eGFP-KRas reporter proteins with C15AlkOPP analog

HEK293 cells were maintained as described above. Upon 80% confluency, 2.5 × 10^5 cells were grown in 2–6-well plates (Corning) for each construct to be transfected, with incubation of each plate for 24 h to allow cells to adhere. Turbofect was then added to each well according to the manufacturer's protocol. C15AlkOPP analog (25 μM) was added 12 h after the addition of Turbofect, and cells were incubated an additional 12 h prior to harvesting. Cells were harvested using gentle scraping in PBS and pelleting at 150 × *g* for 5 min, and cell pellets were stored at −80 °C.

CuAAC reactions on protein lysates

Cell pellets that were metabolically labeled with C15AlkOPP were lysed in lysis buffer (10 mM PO_4^{3-}, 137 mM NaCl, 2.7 mM KCl, 2.4 μM PMSF, 65 units of benzonase nuclease, protease inhibitor mixture), and the protein concentration was determined by BCA assay. For in-gel fluorescence analysis, proteins (100 μg) were subjected to click reaction with TAMRA-N_3 under conditions described above. Proteins were recovered by precipitation (ProteoExtract, Calbiochem), redissolved in 1× Laemmli buffer, and resolved in a 10% SDS-polyacrylamide gel (40 μg of proteins). In-gel fluorescence and Coomassie staining were performed as described above. For biotinylation of C15AlkOPP-labeled protein lysates from HEK293 cells transfected with eGFP-KRas-CMIIM and eGFP-KRas-SMIIM, 2 mg of lysate protein in 1 ml of lysis buffer were reacted with 100 μM biotin-N_3 in the presence of 1 mM TCEP, 0.1 mM tris[(1-benzyl-1*H*-1,2,3-triazol-4-yl)methyl]amine, and 1 mM $CuSO_4$ for 1.5 h at room temperature. Proteins were recovered by precipitation (1× $CHCl_3$, 4× CH_3OH, 3× H_2O) and redissolved in 1 ml of 1× PBS with 1% SDS.

Enrichment and sample preparation for proteomic analysis

The biotinylated protein lysates were incubated with prewashed Neutravidin® (100 μl of beads) for 1.5 h and washed with 1× PBS + 1% SDS (three times), 1× PBS, 8 M urea in 50 mM TEAB (three times), and 50 mM triethylammonium bicarbonate (TEAB) (three times). Proteins were reduced with DTT (10 mM) and alkylated with iodoacetamide (10 mM) followed by digestion with 0.5 μg of sequencing grade trypsin overnight. Tryptic peptides were collected, lyophilized, and redissolved in 100 mM TEAB. Peptides (10 μg) were labeled with TMT duplex (Thermo Fisher Scientific) following the manufacturer's protocol (eGFP-KRas-SMIIM, TMT-126; eGFP-KRas-CMIIM, TMT-127). The TMT-labeled peptides were fractionated under high pH reversed phase conditions on STAGE tips into fractions containing 5, 10, 15, 20, 25, and 80% acetonitrile in 200 mM ammonium formate, pH 10.

LC-MS/MS and data analysis

LC-MS/MS analyses were performed using an RSLCnano system (Dionex) and Orbitrap Elite Hybrid mass spectrometer. Each fraction was fractionated using a column (75 μm inner diameter, 35 cm) manufactured in-house and eluted at 300 nl/min using an 80-min gradient with 0.1% formic acid in water and 0.1% formic acid in acetonitrile. A data-dependent acquisition was performed set at 60,000 resolution over 350–1500 *m/z* range. High-energy collision dissociation (HCD) fragmentation was carried out with 1.4 *m*/*z* isolation window and normalized collision energy (NCE) of 40%. The maximum injection times were 100 and 500 ms, and ion targets were 10^6 and 5 × 10^4 for MS and MS/MS (at 15,000 *m/z* resolution), respectively.

[3] Please note that the JBC is not responsible for the long-term archiving and maintenance of this site or any other third party hosted site.

The .raw files were analyzed with MaxQuant version 1.6.0.16 and searched against non-redundant human proteome database (UP000005640) and common contaminants. Data output was further processed using Perseus version 1.6.0.7 with protein identification based on only identified by site, and reverse sequences and contaminants (except GFP) were removed. A two-sample *t* test was performed across three replicates (FDR = 0.05, s0 = 0.5), and the volcano plot generated was exported to Microsoft Excel for formatting.

Author contributions—M. J. B. performed peptide- and protein-based prenylation assays, designed and expressed protein substrates, performed cell imaging experiments, and prepared metabolic labeling samples. K. F. S. performed mass spectrometry and gel analysis of *in vitro* farnesylated peptides and proteins and proteomic analysis. E. R. H., D. S. H., W. P. S., M. P., and W. K. S. performed the yeast screens and yeast-based biological assays. M. J. B., K. F. S., M. D. D., W. K. S., and J. L. H. designed experiments. M. J. B., K. F. S., M. D. D., W. K. S., and J. L. H. wrote the manuscript.

Acknowledgments—We thank Dr. Avrom Caplan (City College of New York) for anti-Ydj1p primary antibody, and we acknowledge the assistance of Dr. Yingchun Zhao for the use of mass spectrometers (Mass Spectrometry Core Facility of the Masonic Cancer Center at the University of Minnesota). We also thank Ora Furman-Schueler for FlexPepBind calculations.

References

1. Walsh, C. T. (2006) *Posttranslational Modification of Proteins. Expanding Nature's Inventory.* Roberts & Company Publishers, Englewood, CO
2. Casey, P. J. (1994) Lipid modifications of G proteins. *Curr. Opin. Cell Biol.* **6,** 219–225 CrossRef Medline
3. Ganesan, L., and Levental, I. (2015) Pharmacological inhibition of protein lipidation. *J. Membr. Biol.* **248,** 929–941 CrossRef Medline
4. Hentschel, A., Zahedi, R. P., and Ahrends, R. (2016) Protein lipid modifications–more than just a greasy ballast. *Proteomics* **16,** 759–782 CrossRef Medline
5. Martin, D. D., Beauchamp, E., and Berthiaume, L. G. (2011) Post-translational myristoylation: fat matters in cellular life and death. *Biochimie* **93,** 18–31 CrossRef Medline
6. Nadolski, M. J., and Linder, M. E. (2007) Protein lipidation. *FEBS J.* **274,** 5202–5210 CrossRef Medline
7. Resh, M. D. (1999) Fatty acylation of proteins: new insights into membrane targeting of myristoylated and palmitoylated proteins. *Biochim. Biophys. Acta* **1451,** 1–16 CrossRef Medline
8. Resh, M. D. (2006) Trafficking and signaling by fatty-acylated and prenylated proteins. *Nat. Chem. Biol.* **2,** 584–590 CrossRef Medline
9. Resh, M. D. (2013) Covalent lipid modifications of proteins. *Curr. Biol.* **23,** R431–R435 CrossRef Medline
10. Marshall, C. J. (1993) Protein prenylation: a mediator of protein-protein interactions. *Science* **259,** 1865–1866 CrossRef Medline
11. Zhang, F. L., and Casey, P. J. (1996) Protein prenylation: molecular mechanisms and functional consequences. *Annu. Rev. Biochem.* **65,** 241–269 CrossRef Medline
12. Benetka, W., Koranda, M., and Eisenhaber, F. (2006) Protein prenylation: An (almost) comprehensive overview on discovery history, enzymology, and significance in physiology and disease. *Monatsh. Chem.* **137,** 1241 CrossRef
13. Yokoyama, K., Goodwin, G. W., Ghomashchi, F., Glomset, J., and Gelb, M. H. (1992) Protein prenyltransferases. *Biochem. Soc. Trans.* **20,** 489–494 CrossRef Medline
14. Caplin, B. E., Ohya, Y., and Marshall, M. S. (1998) Amino acid residues that define both the isoprenoid and C*AAX* preferences of the *Saccharomyces cerevisiae* protein farnesyltransferase. Creating the perfect farnesyltransferase. *J. Biol. Chem.* **273,** 9472–9479 CrossRef Medline
15. Lamphear, C. L. (2012) Molecular Recognition of Substrates by Protein Farnesyltransferase and Geranylgeranyltransferase-I. Ph.D. thesis, University of Michigan, Ann Arbor, MI
16. Hougland, J. L., Hicks, K. A., Hartman, H. L., Kelly, R. A., Watt, T. J., and Fierke, C. A. (2010) Identification of novel peptide substrates for protein farnesyltransferase reveals two substrate classes with distinct sequence selectivities. *J. Mol. Biol.* **395,** 176–190 CrossRef Medline
17. Hartman, H. L., Hicks, K. A., and Fierke, C. A. (2005) Peptide specificity of protein prenyltransferases is determined mainly by reactivity rather than binding affinity. *Biochemistry* **44,** 15314–15324 CrossRef Medline
18. Guo, Z., Wu, Y. W., Das, D., Delon, C., Cramer, J., Yu, S., Thuns, S., Lupilova, N., Waldmann, H., Brunsveld, L., Goody, R. S., Alexandrov, K., and Blankenfeldt, W. (2008) Structures of RabGGTase-substrate/product complexes provide insights into the evolution of protein prenylation. *EMBO J.* **27,** 2444–2456 CrossRef Medline
19. Khosravi-Far, R., Clark, G. J., Abe, K., Cox, A. D., McLain, T., Lutz, R. J., Sinensky, M., and Der, C. J. (1992) Ras (CXXX) and Rab (CC/CXC) prenylation signal sequences are unique and functionally distinct. *J. Biol. Chem.* **267,** 24363–24368 Medline
20. Shen, F., and Seabra, M. C. (1996) Mechanism of digeranylgeranylation of Rab proteins. Formation of a complex between monogeranylgeranyl-Rab and Rab escort protein. *J. Biol. Chem.* **271,** 3692–3698 CrossRef Medline
21. Wang, M., and Casey, P. J. (2016) Protein prenylation: Unique fats make their mark on biology. *Nat. Rev. Mol. Cell Biol.* **17,** 110–122 CrossRef Medline
22. Lau, H. Y., Tang, J., Casey, P. J., and Wang, M. (2017) Isoprenylcysteine carboxylmethyltransferase is critical for malignant transformation and tumor maintenance by all RAS isoforms. *Oncogene.* **36,** 3934–3942 CrossRef Medline
23. Feig, L. A., and Buchsbaum, R. J. (2002) Cell signaling: Life or death decisions of Ras proteins. *Curr. Biol.* **12,** R259–R261 CrossRef Medline
24. Casey, P. J. (1995) Protein lipidation in cell signaling. *Science* **268,** 221–225 CrossRef Medline
25. Vantaggiato, C., Formentini, I., Bondanza, A., Bonini, C., Naldini, L., and Brambilla, R. (2006) ERK1 and ERK2 mitogen-activated protein kinases affect Ras-dependent cell signaling differentially. *J. Biol.* **5,** 14 CrossRef Medline
26. Michaelson, D., Ali, W., Chiu, V. K., Bergo, M., Silletti, J., Wright, L., Young, S. G., and Philips, M. (2005) Postprenylation C*AAX* processing is required for proper localization of Ras but not Rho GTPases. *Mol. Biol. Cell* **16,** 1606–1616 CrossRef Medline
27. Leung, K. F., Baron, R., Ali, B. R., Magee, A. I., and Seabra, M. C. (2007) Rab GTPases containing a C*AAX* motif are processed post-geranylgeranylation by proteolysis and methylation. *J. Biol. Chem.* **282,** 1487–1497 CrossRef Medline
28. Winter-Vann, A. M., and Casey, P. J. (2005) Post-prenylation-processing enzymes as new targets in oncogenesis. *Nat. Rev. Cancer* **5,** 405–412 CrossRef Medline
29. Gutierrez, L., Magee, A. I., Marshall, C. J., and Hancock, J. F. (1989) Post-translational processing of p21ras is two-step and involves carboxyl-methylation and carboxy-terminal proteolysis. *EMBO J.* **8,** 1093–1098 Medline
30. Solski, P. A., Helms, W., Keely, P. J., Su, L., and Der, C. J. (2002) RhoA biological activity is dependent on prenylation but independent of specific isoprenoid modification. *Cell Growth Differ.* **13,** 363–373 Medline
31. Roberts, P. J., Mitin, N., Keller, P. J., Chenette, E. J., Madigan, J. P., Currin, R. O., Cox, A. D., Wilson, O., Kirschmeier, P., and Der, C. J. (2008) Rho family GTPase modification and dependence on C*AAX* motif-signaled posttranslational modification. *J. Biol. Chem.* **283,** 25150–25163 CrossRef Medline
32. Hildebrandt, E. R., Cheng, M., Zhao, P., Kim, J. H., Wells, L., and Schmidt, W. K. (2016) A shunt pathway limits the C*AAX* processing of Hsp40 Ydj1p and regulates Ydj1p-dependent phenotypes. *eLife* **5,** e15899 Medline

33. Powers, S., Michaelis, S., Broek, D., Santa Anna, S., Field, J., Herskowitz, I., and Wigler, M. (1986) RAM, a gene of yeast required for a functional modification of RAS proteins and for production of mating pheromone a-factor. *Cell* **47,** 413–422 CrossRef Medline
34. Clarke, S., Vogel, J. P., Deschenes, R. J., and Stock, J. (1988) Posttranslational modification of the Ha-ras oncogene protein: Evidence for a third class of protein carboxyl methyltransferases. *Proc. Natl. Acad. Sci. U.S.A.* **85,** 4643–4647 CrossRef Medline
35. Farnsworth, C. C., Wolda, S. L., Gelb, M. H., and Glomset, J. A. (1989) Human lamin B contains a farnesylated cysteine residue. *J. Biol. Chem.* **264,** 20422–20429 Medline
36. Vorburger, K., Kitten, G. T., and Nigg, E. A. (1989) Modification of nuclear lamin proteins by a mevalonic acid derivative occurs in reticulocyte lysates and requires the cysteine residue of the C-terminal CXXM motif. *EMBO J.* **8,** 4007–4013 Medline
37. Kitten, G. T., and Nigg, E. A. (1991) The C*AAX* motif is required for isoprenylation, carboxyl methylation, and nuclear membrane association of lamin B2. *J. Cell. Biol.* **113,** 13–23 CrossRef Medline
38. Hancock, J. F., Magee, A. I., Childs, J. E., and Marshall, C. J. (1989) All Ras proteins are polyisoprenylated but only some are palmitoylated. *Cell* **57,** 1167–1177 CrossRef Medline
39. Schaber, M. D., O'Hara, M. B., Garsky, V. M., Mosser, S. C., Bergstrom, J. D., Moores, S. L., Marshall, M. S., Friedman, P. A., Dixon, R. A., and Gibbs, J. B. (1990) Polyisoprenylation of Ras *in vitro* by a farnesyl-protein transferase. *J. Biol. Chem.* **265,** 14701–14704 Medline
40. Hancock, J. F., Cadwallader, K., Paterson, H., and Marshall, C. J. (1991) A C*AAX* or a CAAL motif and a second signal are sufficient for plasma membrane targeting of ras proteins. *EMBO J.* **10,** 4033–4039 Medline
41. Moores, S. L., Schaber, M. D., Mosser, S. D., Rands, E., O'Hara, M. B., Garsky, V. M., Marshall, M. S., Pompliano, D. L., and Gibbs, J. B. (1991) Sequence dependence of protein isoprenylation. *J. Biol. Chem.* **266,** 14603–14610 Medline
42. Lane, K. T., and Beese, L. S. (2006) Thematic review series: Lipid posttranslational modifications. Structural biology of protein farnesyltransferase and geranylgeranyltransferase type I. *J. Lipid Res.* **47,** 681–699 CrossRef Medline
43. Hougland, J. L., Lamphear, C. L., Scott, S. A., Gibbs, R. A., and Fierke, C. A. (2009) Context-dependent substrate recognition by protein farnesyltransferase. *Biochemistry* **48,** 1691–1701 CrossRef Medline
44. Hougland, J. L., Gangopadhyay, S. A., and Fierke, C. A. (2012) Expansion of protein farnesyltransferase specificity using "tunable" active site interactions: development of bioengineered prenylation pathways. *J. Biol. Chem.* **287,** 38090–38100 CrossRef Medline
45. Reid, T. S., Terry, K. L., Casey, P. J., and Beese, L. S. (2004) Crystallographic analysis of C*AAX* prenyltransferases complexed with substrates defines rules of protein substrate selectivity. *J. Mol. Biol.* **343,** 417–433 CrossRef Medline
46. London, N., Lamphear, C. L., Hougland, J. L., Fierke, C. A., and Schueler-Furman, O. (2011) Identification of a novel class of farnesylation targets by structure-based modeling of binding specificity. *PLoS Comput. Biol.* **7,** e1002170 CrossRef Medline
47. Maurer-Stroh, S., and Eisenhaber, F. (2005) Refinement and prediction of protein prenylation motifs. *Genome Biol.* **6,** R55 CrossRef Medline
48. Maurer-Stroh, S., Koranda, M., Benetka, W., Schneider, G., Sirota, F. L., and Eisenhaber, F. (2007) Towards complete sets of farnesylated and geranylgeranylated proteins. *PLoS Comput. Biol.* **3,** e66 CrossRef Medline
49. Cui, G., Wang, B., and Merz, K. M., Jr. (2005) Computational studies of the farnesyltransferase ternary complex part i: Substrate binding. *Biochemistry* **44,** 16513–16523 CrossRef Medline
50. Caplan, A. J., Tsai, J., Casey, P. J., and Douglas, M. G. (1992) Farnesylation of YDJ1p is required for function at elevated growth temperatures in *Saccharomyces cerevisiae*. *J. Biol. Chem.* **267,** 18890–18895 Medline
51. Kimura, Y., Yahara, I., and Lindquist, S. (1995) Role of the protein chaperone YDJ1 in establishing Hsp90-mediated signal transduction pathways. *Science* **268,** 1362–1365 CrossRef Medline
52. Lu, Z., and Cyr, D. M. (1998) The conserved carboxyl terminus and zinc finger-like domain of the co-chaperone Ydj1 assist Hsp70 in protein folding. *J. Biol. Chem.* **273,** 5970–5978 CrossRef Medline
53. Qiu, X.-B., Shao, Y.-M., Miao, S., and Wang, L. (2006) The diversity of the DnaJ/Hsp40 family, the crucial partners for Hsp70 chaperones. *Cell. Mol. Life Sci.* **63,** 2560–2570 CrossRef Medline
54. Jennings, B. C., Danowitz, A. M., Wang, Y. C., Gibbs, R. A., Distefano, M. D., and Fierke, C. A. (2016) Analogs of farnsyl diphosphate alter C*AAX* substrate specificity and reactions rates of protein farnesyltransferase. *Bioorg. Med. Chem. Lett.* **26,** 1333–1336 CrossRef Medline
55. DeGraw, A. J., Palsuledesai, C., Ochocki, J. D., Dozier, J. K., Lenevich, S., Rashidian, M., and Distefano, M. D. (2010) Evaluation of alkyne-modified isoprenoids as chemical reporters of protein prenylation. *Chem. Biol. Drug Des.* **76,** 460–471 CrossRef Medline
56. Kho, Y., Kim, S. C., Jiang, C., Barma, D., Kwon, S. W., Cheng, J., Jaunbergs, J., Weinbaum, C., Tamanoi, F., Falck, J., and Zhao, Y. (2004) A tagging-via-substrate technology for detection and proteomics of farnesylated proteins. *Proc. Natl. Acad. Sci. U.S.A.* **101,** 12479–12484 CrossRef Medline
57. Chan, R. K., and Otte, C. A. (1982) Isolation and genetic analysis of *Saccharomyces cerevisiae* mutants supersensitive to G_1 arrest by a factor and α factor pheromones. *Mol. Cell. Biol.* **2,** 11–20 CrossRef Medline
58. Firth, A. E., and Patrick, W. M. (2008) GLUE-IT and PEDEL-AA: new programmes for analyzing protein diversity in randomized libraries. *Nucleic Acids Res.* **36,** W281–W285 CrossRef Medline
59. Stirtan, W. G., and Poulter, C. D. (1997) Yeast protein geranylgeranyltransferase type-I: steady-state kinetics and substrate binding. *Biochemistry* **36,** 4552–4557 CrossRef Medline
60. Pickett, W. C., Zhang, F. L., Silverstrim, C., Schow, S. R., Wick, M. M., and Kerwar, S. S. (1995) A fluorescence assay for geranylgeranyl transferase type I. *Anal. Biochem.* **225,** 60–63 CrossRef Medline
61. Cassidy, P. B., Dolence, J. M., and Poulter, C. D. (1995) Continuous fluorescence assay for protein prenyltransferases. *Methods Enzymol.* **250,** 30–43 CrossRef Medline
62. Pompliano, D. L., Gomez, R. P., and Anthony, N. J. (1992) Intramolecular fluorescence enhancement: a continuous assay of Ras farnesyl:protein transferase. *J. Am. Chem. Soc.* **114,** 7945–7946 CrossRef
63. Gangopadhyay, S. A., Losito, E. L., and Hougland, J. L. (2014) Targeted reengineering of protein geranylgeranyltransferase type I selectivity functionally implicates active-site residues in protein-substrate recognition. *Biochemistry* **53,** 434–446 CrossRef Medline
64. Hosokawa, A., Wollack, J. W., Zhang, Z., Chen, L., Barany, G., and Distefano, M. D. (2007) Evaluation of an alkyne-containing analogue of farnesyl diphosphate as a dual substrate for protein-prenyltransferases. *Int. J. Pep. Res. Ther.* **13,** 345–354 CrossRef
65. Subramanian, T., Pais, J. E., Liu, S., Troutman, J. M., Suzuki, Y., Leela Subramanian, K., Fierke, C. A., Andres, D. A., and Spielmann, H. P. (2012) Farnesyl diphosphate analogues with aryl moieties are efficient alternate substrates for protein farnesyltransferase. *Biochemistry* **51,** 8307–8319 CrossRef Medline
66. Zhu, K., Hamilton, A. D., and Sebti, S. M. (2003) Farnesyltransferase inhibitors as anticancer agents: current status. *Curr. Opin. Investig. Drugs* **4,** 1428–1435 Medline
67. Alsina, M., Fonseca, R., Wilson, E. F., Belle, A. N., Gerbino, E., Price-Troska, T., Overton, R. M., Ahmann, G., Bruzek, L. M., Adjei, A. A., Kaufmann, S. H., Wright, J. J., Sullivan, D., Djulbegovic, B., Cantor, A. B., *et al.* (2004) Farnesyltransferase inhibitor tipifarnib is well tolerated, induces stabilization of disease, and inhibits farnesylation and oncogenic/tumor survival pathways in patients with advanced multiple myeloma. *Blood* **103,** 3271–3277 CrossRef Medline
68. Reid, T. S., and Beese, L. S. (2004) Crystal structures of the anticancer clinical candidates R115777 (Tipifarnib) and BMS-214662 complexed with protein farnesyltransferase suggest a mechanism of FTI selectivity. *Biochemistry* **43,** 6877–6884 CrossRef Medline
69. Rashidian, M., Kumarapperuma, S. C., Gabrielse, K., Fegan, A., Wagner, C. R., and Distefano, M. D. (2013) Simultaneous dual protein labeling using a triorthogonal reagent. *J. Am. Chem. Soc.* **135,** 16388–16396 CrossRef Medline

70. Zhang, Y., Blanden, M. J., Sudheer, Ch., Gangopadhyay, S. A., Rashidian, M., Hougland, J. L., and Distefano, M. D. (2015) Simultaneous site-specific dual protein labeling using protein prenyltransferases. *Bioconjug. Chem.* **26,** 2542–2553 CrossRef Medline
71. Rashidian, M., Song, J. M., Pricer, R. E., and Distefano, M. D. (2012) Chemoenzymatic reversible immobilization and labeling of proteins without prior purification. *J. Am. Chem. Soc.* **134,** 8455–8467 CrossRef Medline
72. Palsuledesai, C. C., Ochocki, J. D., Kuhns, M. M., Wang, Y.-C., Warmka, J. K., Chernick, D. S., Wattenberg, E. V., Li, L., Arriaga, E. A., and Distefano, M. D. (2016) Metabolic labeling with an alkyne-modified isoprenoid analog facilitates imaging and quantification of the prenylome in cells. *ACS Chem. Biol.* **11,** 2820–2828 CrossRef Medline
73. Flynn, S. C., Lindgren, D. E., and Hougland, J. L. (2014) Quantitative determination of cellular farnesyltransferase activity: towards defining the minimum substrate reactivity for biologically relevant protein farnesylation. *Chembiochem* **15,** 2205–2210 CrossRef Medline
74. Thissen, J. A., Gross, J. M., Subramanian, K., Meyer, T., and Casey, P. J. (1997) Prenylation-dependent association of Ki-ras with microtubules. Evidence for a role in subcellular trafficking. *J. Biol. Chem.* **272,** 30362–30370 CrossRef Medline
75. Suazo, K. F., Schaber, C., Palsuledesai, C. C., Odom John, A. R., and Distefano, M. D. (2016) Global proteomic analysis of prenylated proteins in *Plasmodium falciparum* using an alkyne-modified isoprenoid analogue. *Sci. Rep.* **6,** 38615 CrossRef Medline
76. Long, S. B., Casey, P. J., and Beese, L. S. (2000) The basis for K-Ras4B binding specificity to protein farnesyltransferase revealed by 2 A resolution ternary complex structures. *Structure* **8,** 209–222 CrossRef Medline
77. Strickland, C. L., Windsor, W. T., Syto, R., Wang, L., Bond, R., Wu, Z., Schwartz, J., Le, H. V., Beese, L. S., and Weber, P. C. (1998) Crystal structure of farnesyl protein transferase complexed with a C*AAX* peptide and farnesyl diphosphate analogue. *Biochemistry* **37,** 16601–16611 CrossRef Medline
78. Turek-Etienne, T. C., Strickland, C. L., and Distefano, M. D. (2003) Biochemical and structural studies with prenyl diphosphate analogues provide insights into isoprenoid recognition by protein farnesyl transferase. *Biochemistry* **42,** 3716–3724 CrossRef Medline
79. Wang, Y.-C., Dozier, J. K., Beese, L. S., and Distefano, M. D. (2014) Rapid analysis of protein farnesyltransferase substrate specificity using peptide libraries and isoprenoid diphosphate analogues. *ACS Chem. Biol.* **9,** 1726–1735 CrossRef Medline
80. Ivanov, S. S., Charron, G., Hang, H. C., and Roy, C. R. (2010) Lipidation by the host prenyltransferase machinery facilitates membrane localization of *Legionella pneumophila* effector proteins. *J. Biol. Chem.* **285,** 34686–34698 CrossRef Medline
81. Hast, M. A., Nichols, C. B., Armstrong, S. M., Kelly, S. M., Hellinga, H. W., Alspaugh, J. A., and Beese, L. S. (2011) Structures of *Cryptococcus neoformans* protein farnesyltransferase reveal strategies for developing inhibitors that target fungal pathogens. *J. Biol. Chem.* **286,** 35149–35162 CrossRef Medline
82. Selvig, K., Ballou, E. R., Nichols, C. B., and Alspaugh, J. A. (2013) Restricted substrate specificity for the geranylgeranyltransferase-I enzyme in *Cryptococcus neoformans*: implications for virulence. *Eukaryot. Cell* **12,** 1462–1471 CrossRef Medline
83. Piispanen, A. E., Bonnefoi, O., Carden, S., Deveau, A., Bassilana, M., and Hogan, D. A. (2011) Roles of Ras1 membrane localization during *Candida albicans* hyphal growth and farnesol response. *Eukaryot. Cell* **10,** 1473–1484 CrossRef Medline
84. Zverina, E. A., Lamphear, C. L., Wright, E. N., and Fierke, C. A. (2012) Recent advances in protein prenyltransferases: substrate identification, regulation, and disease interventions. *Curr. Opin. Chem. Biol.* **16,** 544–552 CrossRef Medline
85. Al-Quadan, T., Price, C. T., London, N., Schueler-Furman, O., and AbuKwaik, Y. (2011) Anchoring of bacterial effectors to host membranes through host-mediated lipidation by prenylation: a common paradigm. *Trends Microbiol.* **19,** 573–579 CrossRef Medline
86. Heilmeyer, L. M., Jr., Serwe, M., Weber, C., Metzger, J., Hoffmann-Posorske, E., and Meyer, H. E. (1992) Farnesylcysteine, a constituent of the α and β subunits of rabbit skeletal muscle phosphorylase kinase: Localization by conversion to *S*-ethylcysteine and by tandem mass spectrometry. *Proc. Natl. Acad. Sci. U.S.A.* **89,** 9554–9558 CrossRef Medline
87. Kilpatrick, E. L., and Hildebrandt, J. D. (2007) Sequence dependence and differential expression of Gγ5 subunit isoforms of the heterotrimeric G proteins variably processed after prenylation in mammalian cells. *J. Biol. Chem.* **282,** 14038–14047 CrossRef Medline
88. Riddles, P. W., Blakeley, R. L., and Zerner, B. (1979) Ellman's reagent: 5,5′-dithiobis(2-nitrobenzoic acid)–a reexamination. *Anal. Biochem.* **94,** 75–81 CrossRef Medline
89. Chen, P., Sapperstein, S. K., Choi, J. D., and Michaelis, S. (1997) Biogenesis of the *Saccharomyces cerevisiae* mating pheromone a-factor. *J. Cell Biol.* **136,** 251–269 CrossRef Medline
90. Michaelis, S., and Herskowitz, I. (1988) The a-factor pheromone of *Saccharomyces cerevisiae* is essential for mating. *Mol. Cell. Biol.* **8,** 1309–1318 CrossRef Medline
91. Krishnankutty, R. K., Kukday, S. S., Castleberry, A. J., Breevoort, S. R., and Schmidt, W. K. (2009) Proteolytic processing of certain C*AAX* motifs can occur in the absence of the Rce1p and Ste24p C*AAX* proteases. *Yeast* **26,** 451–463 CrossRef Medline
92. Schmidt, W. K., Tam, A., and Michaelis, S. (2000) Reconstitution of the Ste24p-dependent N-terminal proteolytic step in yeast a-factor biogenesis. *J. Biol. Chem.* **275,** 6227–6233 CrossRef Medline
93. Sikorski, R. S., and Hieter, P. (1989) A system of shuttle vectors and yeast host strains designed for efficient manipulation of DNA in *Saccharomyces cerevisiae*. *Genetics* **122,** 19–27 Medline
94. Oldenburg, K. R., Vo, K. T., Michaelis, S., and Paddon, C. (1997) Recombination-mediated PCR-directed plasmid construction *in vivo* in yeast. *Nucleic Acids Res.* **25,** 451–452 CrossRef Medline
95. Elble, R. (1992) A simple and efficient procedure for transformation of yeasts. *BioTechniques* **13,** 18–20 Medline
96. Kim, S., Lapham, A. N., Freedman, C. G., Reed, T. L., and Schmidt, W. K. (2005) Yeast as a tractable genetic system for functional studies of the insulin-degrading enzyme. *J. Biol. Chem.* **280,** 27481–27490 CrossRef Medline
97. Rashidian, M., Dozier, J. K., Lenevich, S., and Distefano, M. D. (2010) Selective labeling of polypeptides using protein farnesyltransferase via rapid oxime ligation. *Chem. Commun.* **46,** 8998–9000 CrossRef Medline
98. Studier, F. W. (2005) Protein production by auto-induction in high density shaking cultures. *Protein Expr. Purif.* **41,** 207–234 CrossRef Medline
99. Hunt, M. E., Scherrer, M. P., Ferrari, F. D., and Matz, M. V. (2010) Very bright green fluorescent proteins from the Pontellid copepod *Pontella mimocerami*. *PLoS One* **5,** e11517 CrossRef Medline
100. Chen, Z., Otto, J. C., Bergo, M. O., Young, S. G., and Casey, P. J. (2000) The C-terminal polylysine region and methylation of K-Ras are critical for the interaction between K-Ras and microtubules. *J. Biol. Chem.* **275,** 41251–41257 CrossRef Medline